



Role of Tropical SST Variability on the Formation of Subtropical Dipoles

Yushi Morioka, Sébastien Masson, Pascal Terray, Chloé Prodhomme, Swadhin K. Behera, Yukio Masumoto

► To cite this version:

Yushi Morioka, Sébastien Masson, Pascal Terray, Chloé Prodhomme, Swadhin K. Behera, et al.. Role of Tropical SST Variability on the Formation of Subtropical Dipoles. *Journal of Climate*, 2014, 27 (12), pp.4486-4507. 10.1175/JCLI-D-13-00506.1 . hal-01086698

HAL Id: hal-01086698

<https://hal.science/hal-01086698>

Submitted on 22 Jun 2016

HAL is a multi-disciplinary open access archive for the deposit and dissemination of scientific research documents, whether they are published or not. The documents may come from teaching and research institutions in France or abroad, or from public or private research centers.

L'archive ouverte pluridisciplinaire **HAL**, est destinée au dépôt et à la diffusion de documents scientifiques de niveau recherche, publiés ou non, émanant des établissements d'enseignement et de recherche français ou étrangers, des laboratoires publics ou privés.

Role of tropical SST variability on the formation of subtropical dipoles

Yushi Morioka¹, Sébastien Masson², Pascal Terray², Chloé Prodhomme²,
Swadhin K. Behera¹, and Yukio Masumoto¹

¹*Research Institute for Global Change, JAMSTEC, Yokohama, Japan*

²*LOCEAN-IPSL, Université Pierre et Marie Curie, Paris, France*

Journal of Climate (accepted)

Mar 7, 2014

Corresponding author address: Dr. Yushi Morioka,

Research Institute for Global Change, JAMSTEC,

3173-25, Showamachi, Kanazawa-ku, Yokohama City, Kanagawa, 236-0001, Japan.

E-mail: morioka@jamstec.go.jp

Abstract

Interannual variations of Sea Surface Temperature (SST) in the midlatitudes of the Southern Hemisphere play an important role in the rainfall variability over the surrounding countries by modulating synoptic-scale atmospheric disturbances. These are frequently associated with a northeast-southwest oriented dipole of positive and negative SST anomalies in each oceanic basin, referred to as a subtropical dipole. This study investigates the role of tropical SST variability on the generation of subtropical dipoles by conducting SST-nudging experiments using a coupled general circulation model. In the experiments where the simulated SST in each tropical basin is nudged to the climatology of the observed SST, the subtropical dipoles tend to occur as frequently as the case in which the simulated SST is allowed to freely interact with the atmosphere. It is found that without the tropical SST variability, the zonally elongated atmospheric mode in the mid-high latitudes, called the Antarctic Oscillation (AAO), becomes dominant and the stationary Rossby waves related to the AAO induce the SLP anomalies in the midlatitudes, which, in turn, generate the subtropical dipoles. These results suggest that the tropical SST variability may not be necessary for generating the subtropical dipoles, and hence provide a useful insight into the important role of the AAO in the midlatitude climate variability.

1. Introduction

More than 80 % of the surface area in the Southern Hemisphere is covered by ocean, and the ocean plays a key role in the rainfall over land as moisture sources. Many countries are located in the low-mid latitudes (0° - 50° S), and highly dependent on rain-fed agriculture. In these regions, rainfall variability is strongly linked with climate variability involving the low-mid latitude oceans, and greatly influences the crop yields, infrastructure, and drinking water (e.g. Jury 2002). A large number of studies on the rainfall variability discussed the impacts of the tropical climate variability such as El Niño-Southern Oscillation (ENSO) (Chiew et al. 1998, Grimm et al. 2000, Richard et al. 2000), but recently, much focus has been placed on links with the midlatitude ocean variability (Reason 2001, Robertson et al. 2003, Ummenhofer et al. 2009, Cai and Cowan 2013).

One of the major oceanic factors for the rainfall variability is Sea Surface Temperature (SST). The SST in the midlatitudes seasonally changes due mostly to solar radiation, and reaches its peak during austral summer (December-February). The SST also undergoes a year-to-year variability, which becomes large during austral summer because of a shallow mixed layer and high solar insolation. The interannual SST variation in the midlatitudes is frequently associated with a northeast-southwest oriented dipole of SST anomalies in each oceanic basin, referred to as a subtropical dipole. Behera and Yamagata (2001) first identified this phenomenon in the southern Indian Ocean. Since then, several studies have shown the existence of subtropical dipoles in the South Atlantic (Fauchereau et al. 2003) and South Pacific (Morioka et al. 2013b).

The generation mechanism of the subtropical dipoles has been widely discussed in the

literature (Suzuki et al. 2004, Hermes and Reason 2005, Chiodi and Harrison 2007, Morioka et al. 2010, 2011, 2012). At the beginning, variations in the subtropical high during late austral spring generate a northeast-southwest oriented dipole of latent heat flux anomalies. This induces dipole anomalies of mixed-layer thickness, and modulates warming of the mixed layer by shortwave radiation. This results in the dipole SST anomalies associated with the subtropical dipole during austral summer. Therefore, the variation in the subtropical high is a key factor for generating the subtropical dipole.

However, possible sources of variability in the subtropical high are not fully understood. Huang and Shukla (2006, 2008) and Morioka et al. (2013a) conducted several Coupled General Circulation Model (CGCM) experiments and suggested that not only ENSO but the atmospheric variability in the mid-high latitudes, called the Antarctic Oscillation (AAO; Thompson and Wallace 2000), may be important for inducing the variability of the Mascarene High, hence generating the Indian Ocean Subtropical Dipole (IOSD). Also, in the CGCM experiments by Morioka et al. (2013a), the IOSD occurs even without the SST variability outside the southern Indian Ocean, suggesting a potential role of the local air-sea feedback during the development of the IOSD, which was discussed by Behera and Yamagata (2001). However, the CGCM used in their studies did not include a sea-ice model and there may be some uncertainties in their simulation for the mid-high latitudes climate. In fact, a large number of studies suggested the importance of sea-ice variability in the high-latitude atmospheric variability through changes in the surface albedo and the air temperature (Simmonds and Budd 1991, Hudson and Hewitson 2001, Raphael 2003).

As the dominant atmospheric variability in the Southern Hemisphere, the AAO plays a

key role in the SST, mixed-layer, and sea-ice variability in the extratropics (Sen Gupta and England 2006, Ciasto and Thompson 2008, Screen 2010). Several studies discussed that the AAO is an internal atmospheric variability sustained by the positive feedback between the zonal-mean flow and eddies (Lorenz and Hartmann 2001, Eichelberger and Hartmann 2007). The positive (negative) AAO is driven by the eddy momentum flux convergence/divergence associated with a strong (weak) anticyclonic Rossby wave breaking on the equator side of the midlatitude jet (Gong et al. 2010, Wang and Magnusdottir 2011). In addition, the SST anomalies associated with the AAO thermodynamically affect the atmosphere in the troposphere and contribute to the persistence of the AAO, suggesting an existence of ocean-to-atmosphere feedback (Sen Gupta and England 2007).

Another important driver for the climate variability in the Southern Hemisphere is atmospheric teleconnection associated with the tropical heating anomalies (Lee et al. 2009). In particular, ENSO has significant impacts on the SST anomalies in the extratropics by modulating surface turbulent heat flux and Ekman heat advection (Ciasto and England 2011). The atmospheric response to ENSO has an equivalent barotropic dipole structure of the zonal-mean wind anomalies in the mid-high latitudes and it is also related with the AAO (L'Heureux and Thompson 2006).

In this context, a large number of studies discussed the role of the AAO and ENSO in the SST variability in the extratropical Southern Hemisphere, but little attention has been paid to the SST variability associated with the subtropical dipoles as well as the impacts arising from the other tropical forcing. For example, the interannual SST variability in the tropical Indian Ocean shows either Indian Ocean Basin (IOB; Klein et al. 1999) or Indian Ocean

Dipole (IOD; Saji et al. 1999) modes. Particularly, the IOD induces the atmospheric teleconnection in the Southern Hemisphere (Chan et al. 2008) and plays an important role in the rainfall variability over Australia (Cai et al. 2011, Cai and Rensch 2013). The Atlantic Niño is another such large interannual SST variability in the tropical Atlantic (Zebiak 1993).

Therefore, this study aims to investigate roles of the SST variability in each tropical ocean for generation of the subtropical dipoles in the Southern Hemisphere. For this purpose, we perform a series of SST-nudging experiments by using a CGCM which includes a sea-ice model. The contents of this paper are as follows. In Section 2, we briefly describe CGCM experiments, observational data, and methodology for the atmospheric analysis. In Section 3, we compare characteristics of the subtropical dipoles among the observation and the CGCM experiments. In Section 4, we perform composite analysis to discuss generation of the subtropical dipole among the experiments. The discussion and conclusions are given in Section 5.

2. Model, data, and methodology

2-1. CGCM experiments

The CGCM used in this study is SINTEX-F2 (Masson et al. 2012). The atmospheric component is ECHAM5 (Roeckner et al. 2003), which has 31 vertical levels on a T106 Gaussian grid. The oceanic component is NEMO (Madec 2008), which includes the LIM2 sea ice model (Fichefet et al. 1997) and has ORCA05 horizontal resolution (0.5°) with 31 vertical levels. The atmospheric and oceanic fields are exchanged every 2 hours with no flux correction by means of the OASIS3 coupler (Valcke et al. 2004). For the control run (CTR)

experiment, the SINTEX-F2 is integrated for 110 years, and monthly mean outputs from the last 80 years are used for the analysis.

Using the SINTEX-F2, we conducted three SST-nudging experiments to examine the role of tropical SST variability. Details of each experiment are given in Table 1a. In the FTP experiment, the SST in the tropical Pacific (30°S-30°N) is nudged to climatology of the AVHRR-only Optimum Interpolation SST version 2 data (OISST v2; Reynolds et al. 2007) for the 1982-2010 period. We added a negative feedback ($-2,400 \text{ W m}^{-2} \text{ K}^{-1}$) to the surface heat flux so that the temperature in the upper 50-m mixed layer is restored within 1 day. Within 5 degrees near the boundaries of the SST-nudging area, a Gaussian smoothing is applied. Similarly, the FTIO and FTA experiments were performed in the tropical Indian and Atlantic (30°S-30°N) Oceans, respectively. All of these experiments are integrated for 50 years, and the monthly outputs for the last 30 years are used for the analysis by removing the first 20 years for the oceanic adjustment to the atmospheric forcing.

For an accurate interpretation of the results from the SST-nudging experiments, it should be noted that the surface heat flux correction in the SST-nudging experiments acts to inhibit coupled interactions and variability in the corrected region to a large extent. In other words, the differences between the CTR and each SST-nudging experiment may allow us to deconvolve the impact of the SST variability in each tropical basin onto the subtropical modes of the Southern Hemisphere.

2-2. Data

For comparison, we use the observed monthly mean SST data from the NOAA OISST

v2 (Reynolds et al. 2002). It has a horizontal resolution of $1^\circ \times 1^\circ$ and covers the 1982-2011 period. Similar results are obtained for the different datasets such as the HadISST (Rayner et al. 2003) and ERSST v3 (Smith et al. 2008). We also use the Sea Level Pressure (SLP) and the geopotential height and horizontal winds at 250 hPa from the NCEP/DOE AMIP-II Reanalysis (Reanalysis-2; Kanamitsu et al. 2002). It covers the same period with a horizontal resolution of $2.5^\circ \times 2.5^\circ$. For precipitation, we use the observed data set from CPC Merged Analysis of Precipitation (CMAP; Xie and Arkin 1997). The resolution and analysis period are the same as in the NCEP Reanalysis-2. For all the above datasets, monthly anomalies were calculated after removing the linear trend and the monthly climatology.

2-3. Wave activity flux

We use a wave activity flux to examine propagation pathways of stationary Rossby waves on a zonally varying basic flow in the upper troposphere (Takaya and Nakamura 1997, 2001). It provides a snapshot for three-dimensional propagation of quasi-geostrophic eddies in a phase independent manner and is parallel to their local group velocity. The formulation of the wave activity flux \vec{W}_s is given as follows:

$$\vec{W}_s = \frac{p}{2|\vec{U}|} \begin{pmatrix} U(\psi'^2_x - \psi'\psi'_{xx}) + V(\psi'_x\psi'_y - \psi'\psi'_{xy}) \\ U(\psi'_x\psi'_y - \psi'\psi'_{xy}) + V(\psi'^2_y - \psi'\psi'_{yy}) \\ \frac{f_0^2}{N^2} [U(\psi'_x\psi'_z - \psi'\psi'_{xz}) + V(\psi'_y\psi'_z - \psi'\psi'_{yz})] \end{pmatrix},$$

where p = (pressure/1000hPa), $\vec{U} = (U, V)$ is the horizontal wind, ψ is the streamfunction, f_0 is the Coriolis parameter and N is the buoyancy frequency. Here, $()'$ indicates the deviation from the monthly climatology. The divergence (convergence) of the wave activity

flux corresponds to the generation (dissipation) of the Rossby waves. The wave activity flux, by definition, is based on the quasi-geostrophic approximation so that it is hard to describe the flux near the Equator. Since the Rossby waves are excited by the vorticity perturbation associated with the thermal or orographic forcing (Hoskins and Karoly 1981), here instead, we have used the divergence (convergence) of the horizontal winds in the upper troposphere to describe potential sources of the Rossby waves.

3. Impacts on characteristics of subtropical dipoles

Before discussing characteristics of subtropical dipoles, it is worthwhile examining to what extent the SST variances change among the CGCM experiments. Figure 1 shows the standard deviation of SST anomalies during austral summer. The spatial pattern of the observed SST variance is well simulated in the CTR experiment, although the simulated amplitude is relatively weak. In both the observation and CTR experiment, the ENSO pattern clearly appears in the tropical Pacific, and thus the SST variance is much larger than in the other tropical basins. Besides in the tropical Pacific, the SST in the midlatitudes generally shows a large variability compared to that in the high latitudes and this observed feature is well simulated in the CTR experiment.

Interestingly, in the absence of tropical SST variability (FTP, FTIO, and FTA experiments), the SST variances in the mid-latitudes do not largely change compared to those in the CTR experiment. This suggests that the amplitude of the SST variability in the midlatitudes may not be strongly influenced by the tropical SST variability. Also, in the absence of the SST variability in the tropical Indian and Atlantic Oceans (FTIO and FTA

experiments), the SST variability in the tropical Pacific remarkably increases, suggesting that the SST variability in the tropical Indian and Atlantic may act to suppress the ENSO signal in the CTR experiment. This change in the tropical Pacific is consistent with some CGCM studies (Dommenget et al. 2006, Santoso et al. 2012) but still in contradiction with other studies (Yu et al. 2002, Wu and Kirtman 2004), which need further investigation in a future study. Although the weak SST variability in the tropical Pacific of the CTR experiment, the SST variability in the tropical Pacific for the FTIO and FTA experiments might be closer to the observed SST variability.

To detect the SST variability associated with the subtropical dipoles, like previous studies (Huang and Shukla 2006, Kataoka et al. 2012, Morioka et al. 2012), we performed Empirical Orthogonal Function (EOF) analysis to all months of the area-weighted SST anomalies in each subtropical-to-midlatitude oceanic basin. Here, we used the domain of 40°E-110°E and 15°S-50°S for the IOSD, 60°W-20°E and 15°S-50°S for the South Atlantic subtropical dipole (SASD), and 150°E-70°W and 25°S-50°S for the South Pacific subtropical dipole (SPSD), respectively.

The spatial patterns of EOF modes for each subtropical dipole are shown in Fig. 2, and their corresponding EOF modes and explained variances are given in Tables 1b and c. All of these EOF modes sufficiently separate from the neighboring EOF modes (North et al. 1982), except for the IOSD in the FTP experiment where the first (20.8%) and second EOF (19.1%) are close to each other. Also, it should be noted that the SST-nudging area in the CGCM experiments extends to 30°S, thus overlaps the northeastern pole of the subtropical dipoles, so the IOSD is not defined in the FTIO experiment, in a similar manner for the SASD and SPSP

in the FTA and FTP experiments.

In the observation, the IOSD is detected as the second EOF mode, whereas in the CTR experiment, it is captured by the first EOF mode (Table 1b). The observed northeast-southwest dipole of SST anomalies is simulated in the higher latitude, and this may lead to a moderately high pattern correlation at 0.44. It is found that the first EOF mode in the observation shows a zonal dipole of the SST anomalies and is linked with the IOB. This IOB-related mode is also detected as the second EOF mode in the CTR experiment (figure not shown). Because of the difference in the EOF analyses, the explained variance of the IOSD in the CTR experiment is 24.5 %, larger than that in the observation, 14.2 % (Table 1c). In the FTP and FTA experiments, the IOSD is identified as the first EOF mode with the explained variances similar to that in the CTR experiment. Also, the spatial patterns of the EOF modes for the IOSD resemble that for the CTR experiment (Fig. 2a). This suggests that the IOSD may exist independent of the SST variability in the tropical Pacific or Atlantic Oceans, which will be further discussed in Section 4.

In contrast with the IOSD, the SASD in the observation is detected as the first EOF mode (Table 1b). This mode is also captured in the CTR experiment with a high pattern correlation at 0.75, although the spatial pattern of the EOF mode shows a northeast-southwest oriented dipole, while in the observation, it is associated with a north-south oriented dipole (Fig. 2b). Also, the SASD is identified as the first EOF mode in the FTP and FTIO experiments, and the explained variances are not much different among the experiments (Table 1c). However, the spatial pattern of the EOF mode in the FTP experiment slightly deforms in such a way that the amplitude of the southwestern (northeastern) SST anomaly pole becomes weaker (stronger)

than that in the CTR experiment. This implies that although the SASD can develop without the SST variability in the tropical Pacific or Indian Oceans, the SST variability in the tropical Pacific may have more influences on the SASD.

Similarly as in the case of the IOSD, the SPSD in the observation is captured by the second EOF mode, which is successfully simulated in the CTR experiment (Fig. 2c, Table 1b). The pattern correlation is high at 0.76. The SPSD is also captured as the third EOF mode in the FTIO experiment and as the second EOF mode in the FTA experiment. It is found that the first EOF modes in the observation and the CGCM experiments show the SST variability related to ENSO, whereas in the FTIO experiment, the SST variability in the second EOF mode is associated with the El Niño Modoki (Ashok et al. 2007). The spatial patterns and explained variances of the SPSD are almost similar among these experiments (Fig. 2c and Table 1c). This suggests that the SST variability in the tropical Indian or Atlantic Oceans may not directly influence the occurrence of the SPSD.

The robustness of the subtropical dipoles among the experiments is further examined with regard to the occurrence frequency. Due to the lack of the reliable observations before 1980s in the Southern Hemisphere, in particular, the South Pacific (see Fig. 1 in Morioka et al. 2013b), we defined subtropical dipole events as years when the principal component of the EOF modes during austral summer exceeds 0.8 standard deviation. The list of event years defined in the observation is given in Table 2, and the occurrence frequency of the total positive and negative events are summarized in Table 3. It should be noted that to compare the occurrence frequency in the CTR experiment with those in the sensitivity experiments, the standard deviation is estimated for occurrence frequencies of the 50 different sets of 30-yr

259 outputs in the CTR experiment. The observed occurrence frequency of the IOSD is 48.3 %,
260 whereas in the CTR experiment, the IOSD occurs at 50.6 % close to the observation.
261 Interestingly, the occurrence frequencies in the FTP and FTA experiments do not largely
262 differ from that in the CTR experiment, suggesting that the interannual SST variability
263 associated with the IOSD may not be influenced by the tropical SST variability. Similarly,
264 the occurrence frequencies of the SASD and SPSD in the sensitivity experiments do not
265 largely change compared to that in the CTR experiment, although the FTP experiment in the
266 SASD shows a slight increase in the occurrence frequency.

267 Another important characteristic of the subtropical dipoles is a strong seasonal
268 dependence in such a way that the SST anomalies associated with the subtropical dipoles
269 develop during austral summer. Here, we calculated a standard deviation of principal
270 components of the EOF modes for each month (Fig. 3). Note that the standard deviation for
271 the 50 different sets of 30-yr outputs in the CTR experiment is also estimated. The IOSD in
272 the observation develops from late austral spring and reaches its peak during austral summer
273 (Fig. 3a). Although there are slight differences in the peak month of the IOSD, all CGCM
274 experiments reasonably simulate the strong seasonality in austral summer with comparable
275 amplitudes. Also, both the SASD and the SPSD clearly show a strong seasonality in austral
276 summer (Figs. 3b and c), but for the SASD, there exists a large difference in the peak month
277 and amplitude among the observation and the CGCM experiments. It is found that the
278 difference in the SST climatology between the observation and the model simulation is much
279 larger in the South Atlantic than in the other oceanic basins (figure not shown). This may
280 have a link with the large disparity in its standard deviation (Fig. 3b). These results suggest

that the seasonal phase-locking nature of the subtropical dipoles may not be largely affected by the SST variability in the other tropical oceans.

4. Potential sources for the generation of subtropical dipoles

The above intriguing results about key characteristics of the subtropical dipoles motivate us to further examine the generation of subtropical dipoles with a focus on the variations in the subtropical highs. We conduct a composite analysis and discuss only the case for the positive events, because the physical mechanism and its impact on the rainfall in surrounding countries for the negative events is found to be almost similar but opposite to that for the positive events.

4-1. Indian Ocean subtropical dipole (IOSD)

Figure 4a shows composite SST anomalies during austral summer of the positive IOSD. Here we used the same criteria for definition of the positive IOSD events as discussed in Section 3, and composited 8, 20, 8, and 6 positive events for the observation, and the CTR, FTP, and FTA experiments, respectively. The SST anomalies in the observation and the CTR experiment show a northeast-southwest oriented dipole in the southern Indian Ocean. In the tropical Pacific, the simulated SST anomalies are associated with a strong La Niña, although they are not significant in the observation. The link with La Niña in the CTR experiment is also seen in the FTA experiment. However, in the FTP experiment, the dipole SST anomalies associated with the IOSD exist without the SST variability in the tropical Pacific. Moreover, the dipole SST anomalies in the FTP experiment resemble those in the CTR experiment,

indicating that ENSO may not be necessarily responsible for the occurrence of the IOSD as in the observation, despite of the overemphasized ENSO in the CTR experiment.

Since the dipole SST anomalies during the IOSD are closely linked with the SLP anomalies (Behera and Yamagata 2001), we examine composite SLP anomalies in Fig. 4b. Note that the SLP anomalies are calculated for Nov. (0) - Jan. (1) because of the delayed oceanic response to the atmospheric forcing (Fauchereau et al. 2003). In the reanalysis data, the Mascarene High anomalously strengthens, whereas in the CTR experiment, the strengthening of the Mascarene High occurs in the southern part of its mean state ($\sim 30^\circ\text{S}$) during austral summer of the analysis period, indicating anomalous southward shift of the Mascarene High. In the CTR experiment, the positive SLP anomalies are zonally elongated in the mid-latitudes and are associated with the negative SLP anomalies over Antarctica, suggesting a possible link with the positive AAO. The negative SST anomaly in the tropical Indian Ocean may act to weaken the Hadley Cell and cause the negative SLP anomalies in the subtropical region, but this cannot explain the positive SLP anomalies in the southern Indian Ocean. Although not visible in the reanalysis data, the potential link with the AAO in the CTR experiment is also found in the FTP and FTA experiments, but the zonal elongation of the positive and negative SLP anomalies is much clearer in the FTP experiment.

In order to determine whether the stronger relationship with ENSO and the AAO in the CTR experiment is due to model bias in simulating the variability inside or outside the southern Indian Ocean, the model results have been further projected onto the observed EOF pattern in Fig. 2a, and the resulting time series have been used as an alternative index for the IOSD to compute composites in the model experiments. As expected, the derived SST

anomalies in the CTR experiment compare favorably to the observed ones in the southern Indian Ocean (figure not shown). However, the main differences in the SST and SLP anomalies between the observation and the CTR experiment still remain, especially for the stronger relationship with ENSO and the AAO. This clearly suggests that origins of the biases are probably linked to the overemphasized ENSO and the AAO, not to the fact that the simulated EOF pattern for the IOSD in Fig. 2a is different from the observed one.

To further assess the link with the AAO in the model experiments, we defined the AAO by using the geopotential height in the upper troposphere and calculated the correlation coefficient between the IOSD and the AAO. The first EOF mode of the geopotential height anomalies at 250 hPa in the reanalysis data and the CGCM experiments are associated with zonal circular positive anomalies in the midlatitudes and the negative anomalies over Antarctica, representing the AAO (Fig. 5). The variance explained by the first EOF mode in the CTR experiment (14.0 %) is very close to that in the reanalysis data (15.0 %). The correlation coefficient between the time series of the principal component of the corresponding EOF mode for the AAO during Nov.-Jan. and that for the IOSD during Dec.-Feb. is found to be significantly large at 0.45 in the CTR experiment, although not significant in the reanalysis data (Table 4). As expected, both the FTP and FTA experiments show a significantly high correlation with the AAO, and in particular, the FTP experiment shows higher correlation (0.72) than that in the CTR experiment. The comparison of the CTR and FTP experiments implies that, without the SST variability in the tropical Pacific, the AAO may play more important role in inducing the IOSD (Hermes and Reason 2005, Morioka et al. 2013a).

347 To investigate a physical link with the AAO in the model experiments, we calculated
348 composite anomalies of geopotential height at 250 hPa and wave activity flux during
349 Nov.(0)-Jan.(1) (Fig. 6a). Positive geopotential height anomalies in the southern Indian
350 Ocean are located above the positive SLP anomalies in the reanalysis data and the CTR
351 experiment, representing an equivalent barotropic structure in the troposphere. In the CTR
352 experiment, the positive anomalies are zonally elongated in the midlatitudes and associated
353 with a propagation of stationary Rossby waves from the negative anomalies over Antarctica,
354 suggesting the physical connection with the AAO. A similar feature is also found in the FTP
355 and FTA experiments.

356 To reveal potential sources of the stationary Rossby waves, we analyzed composite
357 anomalies of the velocity potential and divergent winds at 250 hPa and the rainfall during
358 Nov.(0)-Jan.(1) in Figs. 6b, and 7. Both the reanalysis data and the CTR experiment show an
359 anomalous wind divergence west of the Antarctic Peninsula, but there is a large disparity in
360 the western tropical Pacific. In the CTR experiment, anomalous divergence occurs in
361 association with La Niña when the seasonal rainfall enhances in the western tropical Pacific
362 (Fig. 7). The associated diabatic heating acts to generate the Rossby waves propagating along
363 the great circle, generating the Pacific-South American (PSA; Mo and Paegle 2001) like
364 teleconnection pattern in the South Pacific. The anomalous rainfall increase is also found
365 over adjacent countries in the southern Indian Ocean, in particular, southern Africa in the
366 CTR experiment, although not significant in the observation. This may be due to the
367 anomalous moisture supply from the southern Indian Ocean linked with the westward
368 extension of the anomalous Mascarene High (Fig. 4b). On the other hand, the rainfall

increase in Australia may be more related to La Niña in the tropical Pacific.

A similar feature of the wind divergence anomalies can be seen in the FTA experiment associated with the increased rainfall in the western tropical Pacific (Fig. 7). However, in the FTP experiment, the spatial pattern of the wind divergence anomalies resembles that in the reanalysis data (Fig. 6b), except that the anomalous divergence occurs in the tropical Indian Ocean in association with the enhanced rainfall in the region (Fig. 7). A comparison of the reanalysis and the FTP experiment suggests that without the SST variability in the tropical Pacific and associated interferences, the anomalous wind divergences in the upper troposphere of mid-high latitudes may excite the stationary Rossby waves and induce the AAO-related positive SLP anomalies in the southern Indian Ocean.

4-2. South Atlantic subtropical dipole (SASD)

The physical mechanism for the SASD is found to be almost similar to that for the IOSD. Similarly as in the IOSD, we conducted the composite analysis and used 6, 21, 9, and 7 positive events for the observation, and the CTR, FTP, and FTIO experiments, respectively. Composite SST anomalies in the observation and the CTR experiment show a northeast-southwest oriented dipole in the South Atlantic (Fig. 8a). These are associated with the negative SST anomalies in the central tropical Pacific related to La Niña. On the other hand, in the FTP experiment, the dipole SST anomaly pattern slightly deforms in such a way that the northeastern pole of the negative SST anomaly extends to the southwest of South Africa. This is expected from the spatial pattern of the corresponding EOF mode in Fig. 2b. Also, in the FTP and FTIO experiments, the SST anomalies in the tropical Pacific show no

significant signal, implying that ENSO may not be a necessary condition for generating the SASD.

Similarly as in the IOSD, St. Helena High in the reanalysis data and the CTR experiment anomalously strengthens in its southern part of the mean state ($\sim 30^\circ\text{S}$) during austral summer of the analysis period, indicating anomalous southward shift of St. Helena High (Fig. 8b). The positive SLP anomalies do not appear to be directly linked with the SST variability in the tropical Atlantic, because the negative SST anomalies in the region tend to weaken the Hadley Cell and cause the negative SLP anomalies in the subtropical region. Rather, they are associated with the negative (positive) SLP anomalies in the western (eastern) tropical Pacific related to La Niña. Also, over Antarctica, the negative SLP anomalies dominate, indicating a possible link with the positive AAO. On the other hand, the link with the positive AAO is not visible in the FTP and FTIO experiments. In fact, the correlation coefficients between the AAO and the SASD in the reanalysis data and the CTR experiment are significantly high, but those in the FTP and FTIO experiment are not significant (Table 4). This implies that in both FTP and FTIO experiments, there may exist some internal atmospheric processes responsible for generating the positive SLP anomalies in the South Atlantic.

To reveal the physical mechanism on the positive SLP anomalies during the positive SASD, composite anomalies of the geopotential height and wave activity flux at 250 hPa are shown in Fig. 9a. In the reanalysis data, the positive geopotential height anomalies in the South Atlantic are associated with a clear propagation of stationary Rossby waves from the positive anomalies in the South Pacific through the negative anomalies west of the Antarctic Peninsula. A similar propagation of the Rossby waves is found in the CTR experiment.

However, in the FTP experiment, the positive anomalies in the South Atlantic are associated with a propagation of the Rossby waves from the positive anomalies west of Antarctic Peninsula through the negative anomalies over the southern South America. Also, in the FTIO experiment, the positive anomalies in the South Atlantic are associated with the negative anomalies west of Antarctic Peninsula. These suggest that the atmospheric variability west of Antarctic Peninsula may have influence on the positive anomalies in the South Atlantic through the Rossby wave propagation, although no significant link with the AAO is found in the FTP and FTIO experiments.

For potential sources of the stationary Rossby waves, composite anomalies of the velocity potential and divergent winds at 250 hPa in the reanalysis data and the CTR experiment show anomalous wind divergence near the Maritime Continent and New Zealand as well as the Antarctic Peninsula (Fig. 9b). In particular, the anomalous wind divergences over the Maritime Continent are related to the enhanced rainfall associated with La Niña (Fig. 10). The significant rainfall increase is also found over southeast Brazil both in the observation and the CTR experiment, which may be partly related to the strengthening of the St. Helena High supplying more moisture from the South Atlantic (Fig. 8b). Although the spatial patterns of the wind divergence anomalies in the FTP and FTIO experiments resemble that in the CTR experiment, there is a clear difference in the wind divergence anomalies in the midlatitudes. Therefore, in the absence of the SST variability in the tropical Pacific or Indian Oceans, the anomalous wind divergences in the midlatitudes may act to generate the stationary Rossby waves, hence the positive SLP anomalies in the South Atlantic.

Finally, a strong coherence between the SASD and the IOSD is found in the analyzed

results. This intriguing aspect was discussed by Hermes and Reason (2005), suggesting that they are highly correlated under the large-scale atmospheric forcing related to the AAO. In the reanalysis data and the CTR experiment (Figs. 8b and 9a), the stationary Rossby waves clearly propagate from the positive SLP anomalies in the South Atlantic through the negative SLP anomalies over Antarctica to the positive SLP anomalies in the southern Indian Ocean. This suggests that the atmospheric Rossby waves play an important role in physically connecting the SLP anomalies, hence the subtropical dipoles in the two oceans. However, some exceptions are found when some of the IOSDs occur independent of the SASDs and some of the positive SASDs occur in association with the negative IOSDs and vice versa. In these cases, the atmospheric signal related to the AAO is absent and less prominent than the above coherent cases (Hermes and Reason 2005). This may be related to the non-linear behavior of the mid-high latitude atmosphere.

4-3. South Pacific subtropical dipole (SPSD)

The physical mechanism on the generation of the PSD is found not to largely differ from the IOSD and the SASD. Similarly, we performed composite analysis to 7, 18, 9, and 7 positive events for the observation, and the CTR, FTIO, and FTA experiments, respectively. The positive PSDs in the observation and the CTR experiment show slightly east-west oriented dipole of positive and negative SST anomalies in the central South Pacific (Fig. 11a). These are associated with the negative SST anomalies southeast of Australia and the positive SST anomalies west of South America. Interestingly, both the observation and the CTR experiment show an association with La Niña in the tropical Pacific. The similar dipole SST

anomaly is found in the FTIO and FTA experiments, but in the FTA experiment, the SST anomaly in the tropical Pacific is associated with El Niño in the central tropical Pacific. This implies that a phase of ENSO may have nothing to do with the occurrence of the SPSPD.

Composite SLP anomalies in the reanalysis data and the CTR experiment (Fig. 11b) show a wave train of positive and negative SLP anomalies in the central South Pacific, as discussed in Morioka et al. (2013b). The wave train of the SLP anomalies does not seem to be directly linked with the negative SST anomaly in the tropical Pacific, because it acts to cause weakening of the Hadley Cell and hence the negative SLP anomalies in the subtropical region. Rather, associated with the La Niña condition, both the reanalysis and the CTR experiment show positive (negative) SLP anomalies in the eastern (western) tropical Pacific. On the other hand, in the FTIO and FTA experiments, the wave train of the SLP anomalies is associated with the negative SLP anomalies in the midlatitudes and the positive SLP anomalies over Antarctica, indicating a possible link with the negative AAO. Although the correlation coefficients between the SPSPD and the AAO are not significant in the reanalysis data and the CTR experiment, they are significantly negative in the FTIO and FTA experiments.

In the upper troposphere, both the reanalysis data and the CTR experiment clearly show a wave train of positive and negative geopotential height anomalies in the South Pacific (Fig. 12a). They are associated with a propagation of stationary Rossby waves from negative anomalies southeast of Australia, which are partly related to the wave propagation from the negative anomalies in the southern Indian Ocean through the positive anomalies over Antarctica. A similar wave propagation is found in the FTA and FTIO experiments, but the

Rossby waves propagate between the negative anomalies in the midlatitudes and the positive anomalies over Antarctica, indicating a strong connection with the negative AAO.

One of the potential sources of the stationary Rossby waves in the reanalysis data and the CTR experiment may be the anomalous wind divergence in the western tropical Pacific (Fig. 12b). This wind divergence anomaly, although not significant, is related to the enhanced rainfall over the Maritime Continent associated with La Niña (Fig. 13). Another possible source may be the anomalous wind divergence in the southern Indian Ocean for the reanalysis data, as discussed by Morioka et al. (2013b). On the other hand, in the FTIO experiment, anomalous wind divergences significantly occur southwest of Australia as well as in the tropical Indian Ocean, which are related to the anomalous rainfall increase in the southern tropical Indian Ocean (Fig. 13). Since the SST variability is suppressed in the tropical Indian Ocean, the enhanced rainfall may be due to an internal atmospheric variability in the tropical basin. Also, in the FTA experiment, the wind divergence anomaly is found in the central tropical Pacific related to El Niño and also south of South Africa (Fig. 12b). These results suggest that even without the SST variability in the tropical Indian or Atlantic Oceans, anomalous wind divergences in the midlatitudes may act to induce the stationary Rossby waves, hence generate the wave train of the positive and negative SLP anomalies in the South Pacific.

5. Summary and discussion

The role of tropical SST variability in the generation of subtropical dipoles is investigated by conducting a series of CGCM experiments in the tropical oceans and the

results for each subtropical dipole are summarized in the schematic diagram (Fig. 14). The CGCM reasonably reproduces the northeast-southwest oriented dipole of positive and negative SST anomalies associated with the subtropical dipole in each oceanic basin, although there exist some discrepancies for the IOSD due to the overemphasized ENSO and the AAO in the model. In the experiments where the SST variability in each tropical basin is suppressed by nudging the simulated SST to the observed climatology, the subtropical dipoles in each oceanic basin are found to develop in association with the variations in the subtropical highs. Interestingly, the occurrence frequencies of subtropical dipoles as well as their strong seasonality in austral summer do not largely change in most cases of the CGCM experiments. Composite analysis reveals that in the absence of the tropical SST variability, the IOSD and the SPSD are associated with the AAO, whereas the SASD is associated with a wave train of SLP anomalies in the midlatitudes. It is found that the Rossby waves generated in the midlatitudes play an important role in inducing the SLP anomalies, hence generating the subtropical dipoles. The results for the IOSD are consistent with the previous CGCM study by Morioka et al. (2013a), although the link with the AAO is not significant in the composite fields of reanalysis data (Table 4) and our model has a tendency to simulate the IOSD in association with the AAO.

The most intriguing result in this study is that, when the tropical SST variability is suppressed, the AAO plays an important role in the atmospheric variability of the midlatitudes, and is able to induce the SST variability associated with the subtropical dipoles. The extratropical SST response to the AAO and/or ENSO has been widely discussed in the previous literature (Sen Gupta and England 2006, Ciasto and Thompson 2008, Ciasto and

England 2011), but few studies paid attention to the SST variability associated with subtropical dipoles and examined the relative contribution from the AAO and the tropical SST variability to the generation of subtropical dipoles. Our CGCM results suggest that the tropical SST variability acts to suppress or counteract the AAO activity inherently existing in mid-high latitudes. This tendency is clearly seen in the standard deviation of the geopotential height anomalies at 250 hPa during Nov.-Jan. (Fig. 15a). Both the reanalysis data and the CTR experiment show large interannual variations in the mid-high latitudes, which are closely linked with the AAO. Interestingly, the standard deviation over the Antarctica in the FTP and FTA experiments becomes larger than that in the CTR experiment. However, in the FTIO experiment, the amplitude of the standard deviation does not largely change compared to the CTR experiment.

Since the atmospheric variability in the upper troposphere of the mid-high latitudes is also influenced by the atmospheric teleconnection through the rainfall variability induced by the SST variability in the tropical oceans (Cai et al. 2011, Ding et al. 2012), we calculated the standard deviation of the rainfall anomalies in the same season (Fig. 15b). Both the observation and CTR experiment show large rainfall variability in the western tropical Pacific and to a lesser extent in the tropical Indian Ocean. The rainfall variability in these regions is suppressed in the FTP and FTA experiments, but does not largely change in the FTIO experiment. This implies that the atmospheric teleconnection from the western tropical Pacific and the tropical Indian Oceans becomes weaker in the FTP and FTA experiments, and the AAO becomes able to play a major role in the SLP variations of the mid-high latitudes. The difference in the rainfall variability in the experiments may be due to the basin

interactions through the change in the walker circulation related to that in the SST variability (Saravanan and Chang 2000), but this is beyond the scope of this study.

Finally, this study provides much implication for both simulation and prediction of subtropical dipoles. To realistically simulate and accurately predict the subtropical dipoles, it is necessary to represent the AAO signal in the model at least in one season prior to the occurrence of the subtropical dipoles. A previous study by Yuan et al. (2013) suggests that it is difficult to predict the subtropical dipoles that are not associated with ENSO. The AAO, itself, is the internal atmospheric variability sustained by the eddy-mean interaction and exists even without the SST variability (Yamazaki and Shinya 1999, Limpasuvan and Hartmann 1999). However, some studies claim an important role of ocean-to-atmosphere feedback in the AAO (Sen Gupta and England 2007), which is worthwhile to examine in the further CGCM study. In addition, there are external factors such as ozone influencing the AAO activity (Sexton 2001), which are not taken into account in the present study. For the realistic simulation of the AAO and hence the subtropical dipoles, it is necessary to reproduce at least both the oceanic and atmospheric mean states in the mid-high latitudes such as the SST, sea-ice, and westerly jet. In this regard, many efforts are required for realistic simulation and accurate prediction of the AAO to represent the climate variability in the midlatitudes of the Southern Hemisphere.

Acknowledgments

The SINTEX-F2 experiments were performed using HPC resources from GENCI-IDRIS (Grant 2012-x2012016895). We are grateful to three anonymous reviewers

567 for providing helpful comments and suggestions on our original manuscript. Also,
568 constructive comments from Drs. Toshio Yamagata, Jérôme Vialard, Takeshi Izumo, Hugo
569 Dayan, and J. V. Ratnam help improve the manuscript. The first author is supported by a
570 research fellowship from the Japan Society for the Promotion of Science (JSPS).

571

References

- Ashok, K., S. K. Behera, S. A. Rao, H. Weng, and T. Yamagata, 2007: El Niño Modoki and its possible teleconnection. *J. Geophys. Res.*, **112**, C11007, doi: 10.1029/2006JC003798
- Behera, S. K., and T. Yamagata, 2001: Subtropical SST dipole events in the southern Indian Ocean. *Geophys. Res. Lett.*, **28**, 327-330.
- Cai, W., P. V. Rensch, T. Cowan, H. H. Hendon, 2011: Teleconnection pathways of ENSO and the IOD and the mechanisms for impacts on Australian rainfall. *J. Climate*, **24**, 3910-3923, doi: 10.1175/2011JCLI4129.1.
- Cai, W., and T. Cowan, 2013: Southeast Australia autumn rainfall reduction: a climate-change-induced poleward shift of ocean-atmosphere circulation. *J. Climate*, **26**, 189-205, doi: 10.1175/JCLI-D-12-00035.1.
- Cai, W., and P. V. Rensch, 2013: Austral summer teleconnections of Indo-Pacific variability: their nonlinearity and impacts on Australian climate. *J. Climate*, **26**, 2796-2810, doi: 10.1175/JCLI-D-12-00458.1.
- Chan, S. C., S. K. Behera, and T. Yamagata, 2008: Indian Ocean Dipole influence on South American rainfall. *Geophys. Res. Lett.*, **35**, L14S12, doi:10.1029/2008GL034204.
- Chiodi, A. M., and D. E. Harrison, 2007: Mechanisms of summertime subtropical southern Indian Ocean sea surface temperature variability: on the importance of humidity anomalies and the meridional advection of water vapor. *J. Climate*, **20**, 4835-4852, doi: 10.1175/JCLI4271.1.
- Chiew, F. H. S., T. C. Piechota, J. A. Dracup, and T. A. McMahon, 1998: El Nino/Southern

594 Oscillation and Australian rainfall, streamflow and drought: Links and potential for
595 forecasting. *J. Hydrology*, **204**, 138-149.

596 Ciasto, L. M., and D. W. J. Thompson, 2008: Observations of large-scale ocean-atmosphere
597 interaction in the Southern Hemisphere. *J. Climate*, **21**, 1244-1259, doi:
598 10.1175/2007JCLI1809.1.

599 Ciasto, L. M., and M. H. England, 2011: Observed ENSO teleconnections to Southern Ocean
600 SST anomalies diagnosed from a surface mixed layer heat budget. *Geophys. Res. Lett.*,
601 **38**, L09701, doi:10.1029/2011GL046895.

602 Ding, Q., E. J. Steig, D. S. Battisti, and J. M. Wallace, 2012: Influence of the tropics on the
603 Southern Annular Mode. *J. Climate*, **25**, 6330-6348, doi: 10.1175/JCLI-D-11-00523.1.

604 Dommenget, D., V. Semenov, and M. Latif, 2006: Impacts of the tropical Indian and Atlantic
605 Oceans on ENSO. *Geophys. Res. Lett.*, **33**, L11701, doi: 10.1029/2006GL025871.

606 Eichelberger, S. J., and D. L. Hartmann, 2007: Zonal jet structure and the leading mode of
607 variability, *J. Climate*, **20**, 5149-5163, doi: 10.1175/JCLI4279.1.

608 Fauchereau, N., S. Trzaska, Y. Richard, P. Roucou, and P. Camberlin, 2003: Sea-surface
609 temperature co-variability in the southern Atlantic and Indian Oceans and its
610 connection with the atmospheric circulation in the Southern Hemisphere. *Int. J.*
611 *Climatol.*, **23**, 663-677, doi: 10.1002/joc.905.

612 Fichet, T., M. A. Morales Maqueda, 1997: Sensitivity of a global sea ice model to the
613 treatment of ice thermodynamics and dynamics. *J. Geophys. Res.*, **102**, C6,
614 12609-12646.

615 Gong, T., S. B. Feldstein, and D. Luo, 2010: The impact of ENSO on wave breaking and

616 Southern Annular Mode events. *J. Atmos. Sci.*, **67**, 2854-2870, doi:
617 10.1175/2010JAS3311.1.

618 Grimm, A. M., V. R. Barros, and M. E. Doyle, 2000: Climate variability in the southern South
619 America associated with El Niño and La Niña Events. *J. Climate*, **13**, 35-58.

620 Hermes, J. C., and C. J. C. Reason, 2005: Ocean model diagnosis of interannual coevolving
621 SST variability in the South Indian and South Atlantic Oceans. *J. Climate*, **18**,
622 2864-2882.

623 Hoskins, B. J., and D. J. Karoly, 1981: The steady linear response of a spherical atmosphere
624 to thermal and orographic forcing. *J. Atmos. Sci.*, **38**, 1179-1196.

625 Huang, B., and J. Shukla, 2006: Interannual SST variability in the southern subtropical and
626 extratropical ocean. *COLA Tech. Rep.*, **223**, 20pp.

627 Huang, B., and J. Shukla, 2008: Interannual variability of the South Indian Ocean in
628 observations and a coupled model. *Indian Journal of Marine Sciences*, **37**, 13-34.

629 Hudson, D. A., and B. C. Hewitson, 2001: The atmospheric response to a reduction in
630 summer Arctic sea-ice extent. *Clim. Res.*, **16**, 79-99.

631 Jury, M. R., 2002: Economic impacts of climate variability in South Africa and development
632 of resource prediction models. *J. Appl. Meteor.*, **41**, 46-55.

633 Kanamitsu, M., W. Ebisuzaki, J. Woollen, S. K. Yang, J. J. Hnilo, M. Fiorino, and G. L.
634 Potter, 2002: NCEP-DOE AMIP-II Reanalysis (R-2). *Bull. Amer. Meteor. Soc.*, **83**,
635 1631-1643, doi: 10.1175/BAMS-83-11-1631.

636 Kataoka, T., T. Tozuka, Y. Masumoto, and T. Yamagata, 2012: The Indian Ocean subtropical
637 dipole mode simulated in the CMIP3 models. *Clim. Dyn.*, **39**, 1385-1399, doi:

638 10.1007/s00382-011-1271-2.

639 Klein, S. A., B. J. Soden, and N.-C. Lau, 1999: Remote sea surface temperature variations
640 during ENSO: evidence for a tropical atmosphere bridge. *J. Climate*, **12**, 917-932.

641 Lee, S. K., C. Wang, and B. E. Mapes, 2009: A simple atmospheric model of the local and
642 teleconnection responses to tropical heating anomalies. *J. Climate*, **22**, 272-284, doi:
643 10.1175/2008JCLI2303.1.

644 L'Heureux, M. L., and D. W. J. Thompson, 2006: Observed relationships between the El
645 Niño-Southern Oscillation and the extratropical zonal-mean circulation. *J. Climate*, **19**,
646 276-287.

647 Limpasuvan, V., and D. L. Hartmann, 1999: Eddies and the annular modes of climate
648 variability. *Geophys. Res. Lett.*, **26**, 3133-3136.

649 Lorenz, D. J., and D. L. Hartmann, 2001: Eddy-zonal flow feedback in the Southern
650 Hemisphere. *J. Atmos. Sci.*, **58**, 3312-3327.

651 Madec, G., 2008: NEMO ocean engine, *Note du Pôle de Modélisation*, Institut Pierre-Simon
652 Laplace (IPSL), France, No 27. ISSN No 1288-1619.

653 Masson, S., P. Terray, G. Madec, J. J. Luo, T. Yamagata, and K. Takahashi, 2012: Impact of
654 intra-daily SST variability on ENSO characteristics in a coupled model. *Clim. Dyn.*, **39**,
655 681-707, doi: 10.1007/s00382-011-1247-2.

656 Mo, K. C., and J. N. Paegle, 2001: The Pacific-South American mode and their downstream
657 effects. *Int. J. Climatol.*, **21**, 1211-1229, doi: 10.1002/joc.685.

658 Morioka, Y., T. Tozuka, and T. Yamagata, 2010: Climate variability in the southern Indian
659 Ocean as revealed by self-organizing maps. *Clim. Dyn.*, **35**, 1059-1072, doi:

10.1007/s00382-010-0843-x.

Morioka, Y., T. Tozuka, and T. Yamagata, 2011: On the growth and decay of the subtropical dipole mode in the South Atlantic. *J. Climate*, **24**, 5538-5554, doi: 10.1175/2011JCLI4010.1.

Morioka, Y., T. Tozuka, S. Masson, P. Terray, J. J. Luo, and T. Yamagata, 2012: Subtropical dipole modes simulated in a coupled general circulation model. *J. Climate*, **25**, 4029-4047, doi: 10.1175/JCLI-D-11-00396.1.

Morioka, Y., T. Tozuka, and T. Yamagata, 2013a: How is the Indian Ocean Subtropical Dipole excited? *Clim. Dyn.*, **41**, 1955-1968, doi: 10.1007/s00382-012-1584-9.

Morioka, Y., J. V. Ratnam, W. Sasaki, and Y. Masumoto, 2013b: Generation mechanism of the South Pacific subtropical dipole. *J. Climate*, **26**, 6033-6045, doi: 10.1175/JCLI-D-12-00648.1.

North, G. R., T. L. Bell, R. F. Cahalan, and F. J. Moeng, 1982: Sampling errors in the estimation of empirical orthogonal functions. *Mon. Wea. Rev.*, **110**, 699-706.

Raphael, M. N., 2003: Impact of observed sea-ice concentration on the Southern Hemisphere extratropical atmospheric circulation in summer. *J. Geophys. Res.*, **108**, D22, 4687, doi: 10.1029/2002JD003308.

Rayner, N. A., D. E. Parker, E. B. Horton, C. K. Folland, L. V. Alexander, D. P. Rowell, E. C. Kent, and A. Kaplan, 2003: Global analyses of sea surface temperature, sea ice, and night marine air temperature since the late nineteenth century. *J. Geophys. Res.*, **108**, D14, 4407, doi: 10.1029/2002JD002670.

Reason, C. J. C., 2001: Subtropical Indian Ocean SST dipole events and southern African

682 rainfall. *Geophys. Res. Lett.*, **28**, 2225-2227.

683 Reynolds, R. W., N. A. Rayner, T. M. Smith, D. C. Stokes, and W. Wang, 2002: An improved
684 in situ and satellite SST analysis for climate. *J. Climate*, **15**, 1609-1625.

685 Reynolds, R. W., T. M. Smith, C. Liu, D. B. Chelton, K. S. Casey, and M. G. Schlax, 2007:
686 Daily high-resolution blended analyses for sea surface temperature. *J. Climate*, **20**,
687 5473-5496, doi: 10.1175/2007JCLI1824.1.

688 Richard, Y., S. Trzaska, P. Roucou, and M. Rouault, 2000: Modification of the southern
689 African rainfall variability/ENSO relationship since the late 1960s. *Clim. Dyn.*, **16**,
690 883-895.

691 Robertson, A. W., J. D. Farrara, and C. R. Mechoso, 2003: Simulations of the atmospheric
692 response to South Atlantic sea surface temperature anomalies. *J. Climate*, **16**,
693 2540-2551.

694 Roeckner, E., and Coauthors, 2003: The atmospheric general circulation model ECHAM5:
695 Part I: model description. Max-Planck-Institut für Meteorologie, Hamburg,
696 MPI-Report 349.

697 Saji, N. H., B. N. Goswami, P. N. Vinayachandran, and T. Yamagata, 1999: A dipole mode in
698 the tropical Indian Ocean. *Nature*, **401**, 360-363.

699 Santoso, A., M. H. England, and W. Cai, 2012: Impact of Indo-Pacific feedback interactions
700 on ENSO dynamics diagnosed using ensemble climate simulations. *J. Climate*, **25**,
701 7743-7763.

702 Saravanan, R., and P. Chang, 2000: Interaction between tropical Atlantic variability and El
703 Niño-Southern Oscillation. *J. Climate*, **13**, 2177-2194.

704 Screen J. A., N. P. Gillett, A. Y. Karpechko, and D. P. Stevens, 2010: Mixed layer
 705 temperature response to the Southern Annular Mode: mechanisms and model
 706 representation. *J. Climate*, **23**, 664-678, doi: 10.1175/2009JCLI2976.1.

707 Sen Gupta, A. and M. H. England, 2006: Coupled ocean-atmosphere-ice response to
 708 variations in the Southern Annular mode. *J. Climate*, **19**, 4457-4486.

709 Sen Gupta, A. and M. H. England, 2007: Coupled ocean-atmosphere feedback in the Southern
 710 Annular Mode. *J. Climate*, **20**, 3677-3692, doi: 10.1175/JCLI4200.1.

711 Sexton, D. M. H., 2001: The effect of stratospheric ozone depletion on the phase of the
 712 Antarctic Oscillation. *Geophys. Res. Lett.*, **28**, 3697-3700.

713 Simmonds, I., and W. F. Budd, 1991: Sensitivity of the Southern Hemisphere circulation to
 714 leads in the Antarctic pack ice. *Q. J. R. Meteorol. Soc.*, **117**, 1003-1024.

715 Smith, T.M., R.W. Reynolds, T. C. Peterson, and J. Lawrimore, 2008: Improvements to
 716 NOAA's historical merged land-ocean surface temperature analysis (1880-2006). *J.*
 717 *Climate*, **21**, 2283-2296.

718 Suzuki, R., S. K. Behera, S. Iizuka, T. Yamagata, 2004: Indian Ocean subtropical dipole
 719 simulated using a coupled general circulation model. *J. Geophys. Res.*, **109**, C09001,
 720 doi: 10.1029/2003JC001974.

721 Takaya, K., and H. Nakamura, 1997: A formulation of a wave-activity flux for stationary
 722 Rossby waves on a zonally varying basic flow. *Geophys. Res. Lett.*, **24**, 2985-2988.

723 Takaya, K., and H. Nakamura, 2001: A formulation of a phase-independent wave-activity
 724 flux for stationary and migratory quasigeostrophic eddies on a zonally varying basic
 725 flow. *J. Atmos. Sci.*, **58**, 608-627.

726 Thompson, D. W. J., and J. M. Wallace, 2000: Annular modes in the extratropical circulation.
727 Part I: month-to-month variability. *J. Climate*, **13**, 1000-1016.

728 Ummenhofer, C. C., A. S. Gupta, A. S. Taschetto, and M. H. England, 2009: Modulation of
729 Australian precipitation by meridional gradients in East Indian Ocean sea surface
730 temperature. *J. Climate*, **22**, 5597-5610, doi: 10.1175/2009JCLI3021.1.

731 Valcke, S., A. Caubel, R. Vogelsang, and D. Declat, 2004: OASIS3 ocean atmosphere sea ice
732 soil user's guide. *Tech. Rep. TR/CMGC/04/68*, CERFACS, Toulouse, France.

733 Wu, R., and B. P. Kirtman, 2004: Understanding the impacts of the Indian Ocean on ENSO
734 variability in a coupled GCM. *J. Climate*, **17**, 4019-4031.

735 Wang, Y. H., and G. Magnusdottir, 2011: Tropospheric Rossby wave breaking and the SAM.
736 *J. Climate*, **24**, 2134-2146, doi: 10.1175/2010JCLI4009.1.

737 Xie, P., and P. A. Arkin, 1997: Analyses of global monthly precipitation using gauge
738 observations, satellite estimates, and numerical model predictions. *J. Climate*, **9**,
739 840-858.

740 Yamazaki, K., and Y. Sinya, 1999: Analysis of the Arctic Oscillation simulated by AGCM. *J.*
741 *Meteor. Soc. Japan*, **77**, 1287-1298.

742 Yu, J. Y., C. R. Mechoso, J. C. McWilliams, and A. Arakawa, 2002: Impacts of the Indian
743 Ocean on the ENSO cycle. *Geophys. Res. Lett.*, **29**, doi: 10.1029/2001GL014098

744 Yuan, C., T. Tozuka, J. J. Luo, and T. Yamagata, 2013: Predictability of the subtropical
745 dipole modes in a coupled ocean-atmosphere model. *Clim. Dyn.*, doi:
746 10.1007/s00382-013-1704-1.

747 Zebiak, S. E., 1993: Air-sea interaction in the equatorial Atlantic region. *J. Climate*, **6**,

748 1567-1586.

749

Tables

Table 1: (a) Details of CGCM experiments performed in this study. (b) EOF modes of SST anomalies in each subtropical-to-midlatitude oceanic basin to define the IOSD, SASD, and SPSD for the observation (OISST) and CGCM (CTR, FTP, FTIO, and FTA) experiments. (c) Explained variances (in %) for the corresponding EOF mode in (b).

(a) CGCM experiments

	SST nudging area	Analysis period
CTR	None	80 yr
FTP	Tropical Pacific (30°S-30°N)	30 yr
FTIO	Tropical Indian (30°S-30°N)	30 yr
FTA	Tropical Atlantic (30°S-30°N)	30 yr

(b) EOF mode

	OISST	CTR	FTP	FTIO	FTA
IOSD	2	1	1		1
SASD	1	1	1	1	
SPSD	2	2		3	2

(c) Explained variance %

	OISST	CTR	FTP	FTIO	FTA
IOSD	14.2	24.5	20.8		25.8
SASD	20.6	19.0	23.1	21.5	
SPSD	13.2	11.8		11.1	12.3

757 **Table 2:** Observed event years for the IOSD, SASD, and SPSD. Pos (Neg) corresponds to
 758 positive (negative) events.

Event years	
	IOSD
Pos	1986, 1987, 1992, 1998, 2003, 2005, 2006, 2010
Neg	1982, 1989, 1991, 1995, 1999, 2002
	SASD
Pos	1989, 1996, 1999, 2001, 2008, 2010
Neg	1982, 1987, 1997, 2000, 2002, 2009
	SPSD
Pos	1983, 1984, 1987, 2001, 2003, 2005, 2008
Neg	1986, 1990, 1994, 1997, 2009, 2010

759

760

761

Table 3: Occurrence frequency (in %) of the IOSD, SASD, and SPSP for the observation (OISST) and CGCM (CTR, FTP, FTIO, and FTA) experiments. Both the positive and negative events are counted together. The values in the parenthesis of the CTR experiment indicate one standard deviation calculated from 50 different sets of 30-yr outputs.

Occurrence frequency					%
	OISST	CTR	FTP	FTIO	FTA
IOSD	48.3	50.6 (± 5.8)	48.3		51.7
SASD	41.4	50.6 (± 6.2)	58.6	48.3	
SPSD	44.8	49.4 (± 10.3)		58.6	55.2

Table 4: Correlation coefficients among the IOSD, SASD, and SPSD indices during Dec.-Feb. and the AAO index during Nov.-Jan. for the NCEP Reanalysis-2 (NCEP2) data and CGCM (CTR, FTP, FTIO, and FTA) experiments. The asterisk indicates a correlation coefficient exceeding 90 % (95 %) confidence level by the two-tailed t-test for the NCEP2 and FTP, FTIO, and FTA experiments (CTR experiment).

Correlation with AAO					
	NCEP2	CTR	FTP	FTIO	FTA
IOSD	0.16	0.45*	0.72*		0.54*
SASD	0.67*	0.39*	-0.28	-0.17	
SPSD	0.22	-0.22		-0.42*	-0.60*

Figure captions

Figure 1: Standard deviation (in °C) of SST anomalies during austral summer for (a) the observation (OISST) and (b) the CGCM CTR experiment. (c-e) As in (b), but for the FTP, FTIO, and FTA experiments, respectively.

Figure 2: (a) Spatial patterns (in °C) of the EOF modes for the IOSD defined in Table 1b. (b-c) As in (a), but for the SASD and SPSD, respectively. Positive values are shaded.

Figure 3: (a) Monthly standard deviation of the principal component of the corresponding EOF modes for the IOSD defined in Table 1b. The red shade in the CTR experiment indicates one standard deviation calculated from 50 different sets of 30-yr outputs. (b-c) As in (a), but for the SASD and SPSD, respectively.

Figure 4: (a) Composite anomalies of SST (in °C) during austral summer of the positive IOSD for the observation (OISST) and CGCM (CTR, FTP, and FTA) experiments. (b) As in (a), but for the SLP (in hPa) during Nov.(0)-Jan.(1). For comparison, NCEP Reanalysis-2 (NCEP2) are shown. Anomalies exceeding the 90% (95%) confidence level by two-tailed t-test are shown for the observation, FTP, and FTA experiments (CTR experiment).

Figure 5: Spatial patterns of the first EOF mode of the geopotential height anomalies at 250 hPa (contour interval is 10 m). The NCEP Reanalysis-2 (NCEP2), the CGCM (CTR, FTP, FTIO, and FTA) experiments are shown, respectively. The positive values are shaded. Values on the top of the panel indicate the explained variance.

Figure 6: (a) As in Fig. 4b, but for the geopotential height at 250 hPa (color, in m) and wave activity flux (arrow, in $\text{m}^2 \text{s}^{-2}$). (b) As in (a), but for the velocity potential at 250 hPa (color, in $10^6 \text{m}^2 \text{s}^{-1}$) and divergent wind (arrow, in m s^{-1}).

Figure 7: As in Fig. 4b, but for the rainfall (color, in mm month⁻¹).

Figure 8: As in Fig. 4, but for the positive SASD. The FTP and FTIO experiments are shown.

Figure 9: As in Fig. 6, but for the positive SASD. The FTP and FTIO experiments are shown.

Figure 10: As in Fig. 7, but for the positive SASD. The FTP and FTIO experiments are shown.

Figure 11: As in Fig. 4, but for the positive SPSD. The FTIO and FTA experiments are shown.

Figure 12: As in Fig. 6, but for the positive SPSD. The FTIO and FTA experiments are shown.

Figure 13: As in Fig. 7, but for the positive SPSD. The FTIO and FTA experiments are shown.

Figure 14: Schematic diagram illustrating the generation mechanism of the IOSD, SASD, and SPSD derived from the reanalysis data and the CTR experiment. The warm (cold) color indicates the positive (negative) SST anomalies and the black shade indicates the anomalous wind divergence in the upper troposphere as possible sources of the Rossby waves. The dashed line shows the propagation pathway of the anomalous high (H) and low (L) pressure in the upper troposphere.

Figure 15: As in Fig. 1, but for (a) geopotential height at 250 hPa (in m) during Nov.-Jan.. (b) As in (a), but for the precipitation (in mm month⁻¹).

819 **Figures**

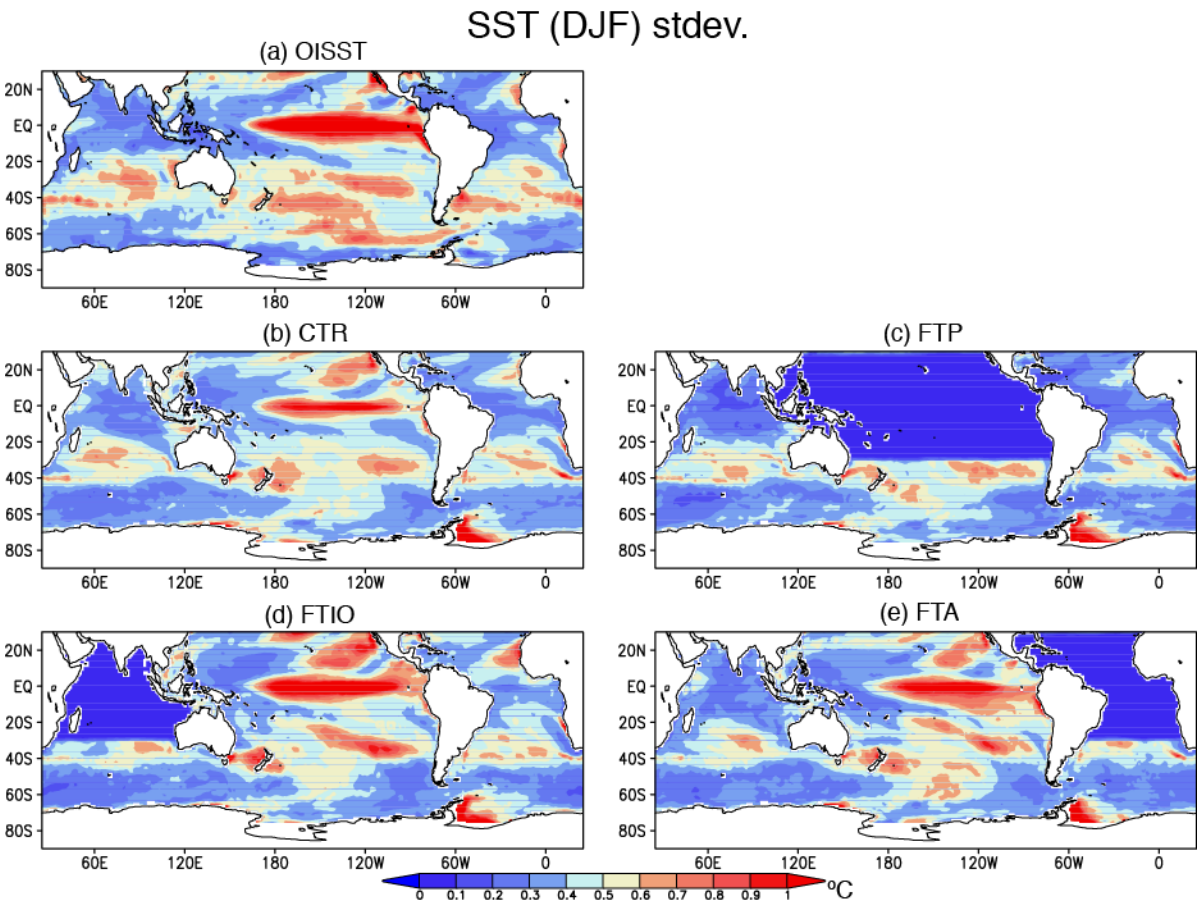
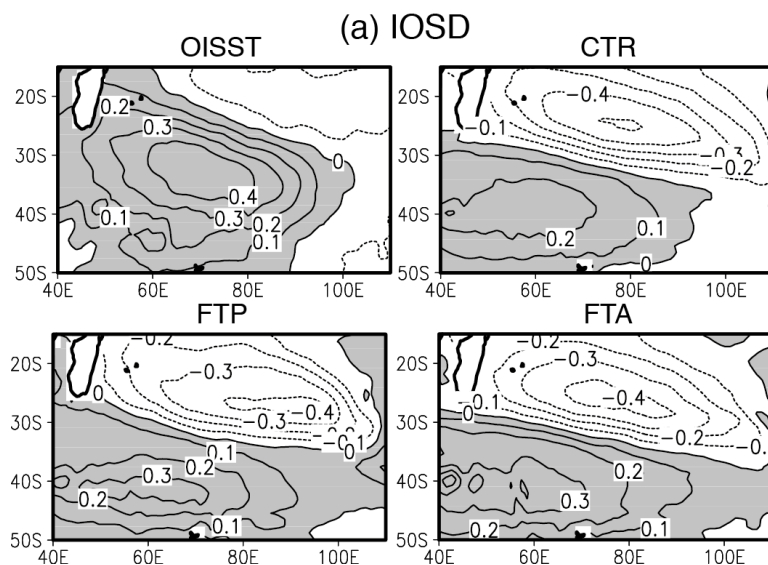
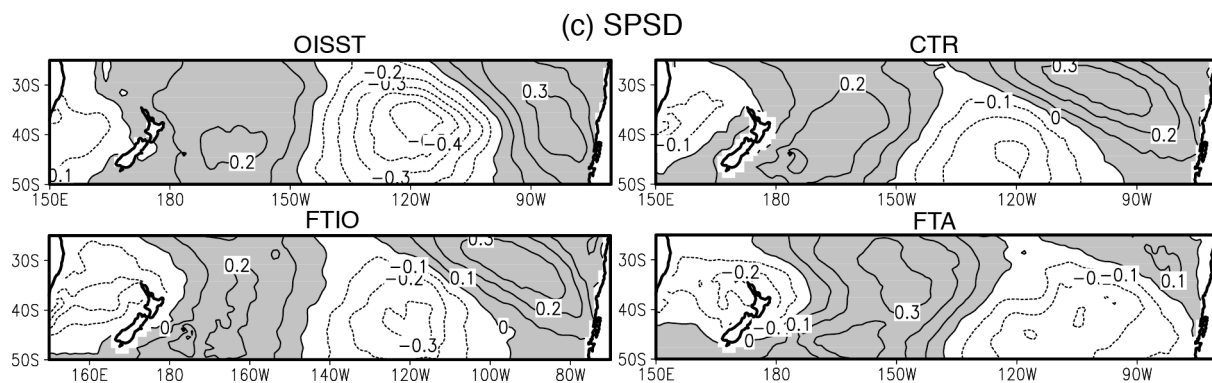
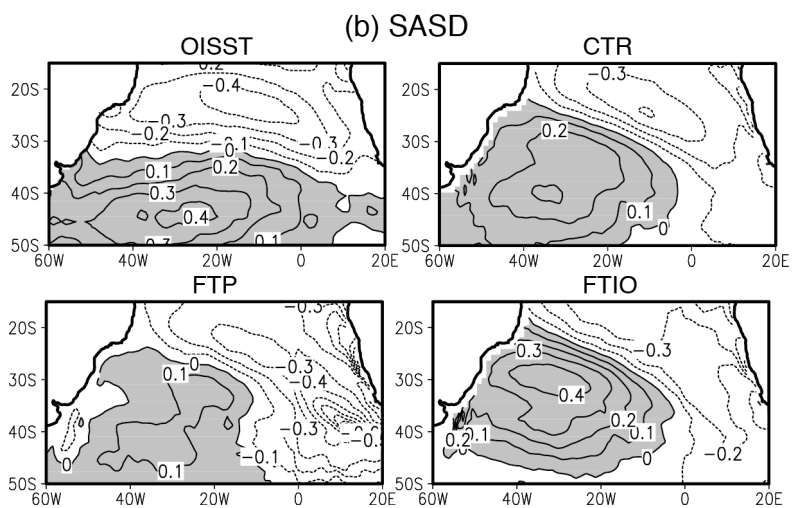


Figure 1: Standard deviation (in °C) of SST anomalies during austral summer for (a) the observation (OISST) and (b) the CGCM CTR experiment. (c-e) As in (b), but for the FTP, FTIO, and FTA experiments, respectively.

825



826



827

828 **Figure 2:** (a) Spatial patterns (in $^{\circ}\text{C}$) of the EOF modes for the IOSD defined in Table 1b.

829 (b-c) As in (a), but for the SASD and SPSP, respectively. Positive values are shaded.

830

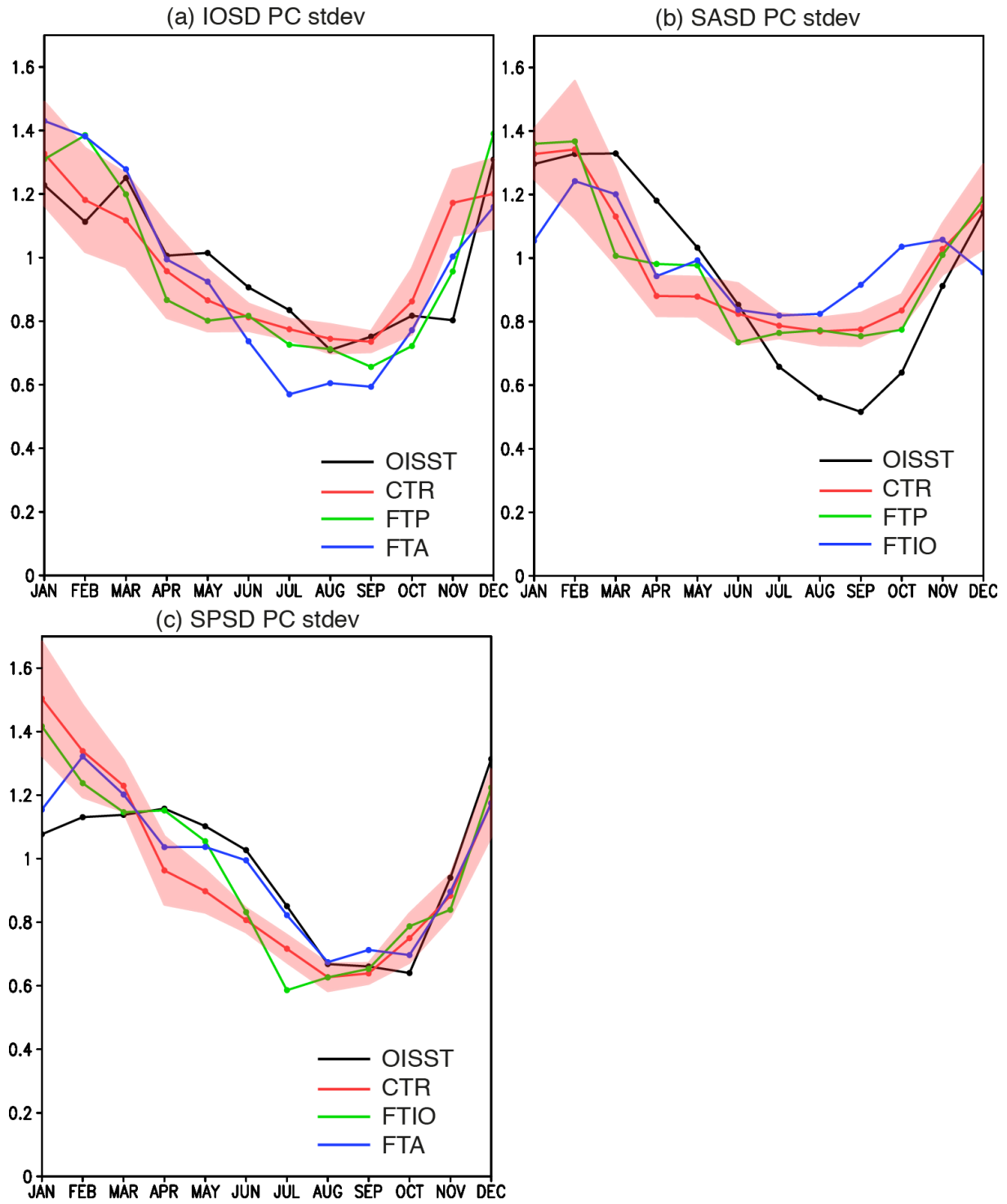


Figure 3: (a) Monthly standard deviation of the principal component of the corresponding EOF modes for the IOSD defined in Table 1b. The red shade in the CTR experiment indicates one standard deviation calculated from 50 different sets of 30-yr outputs. (b-c) As in (a), but for the SASD and SPSSD, respectively.

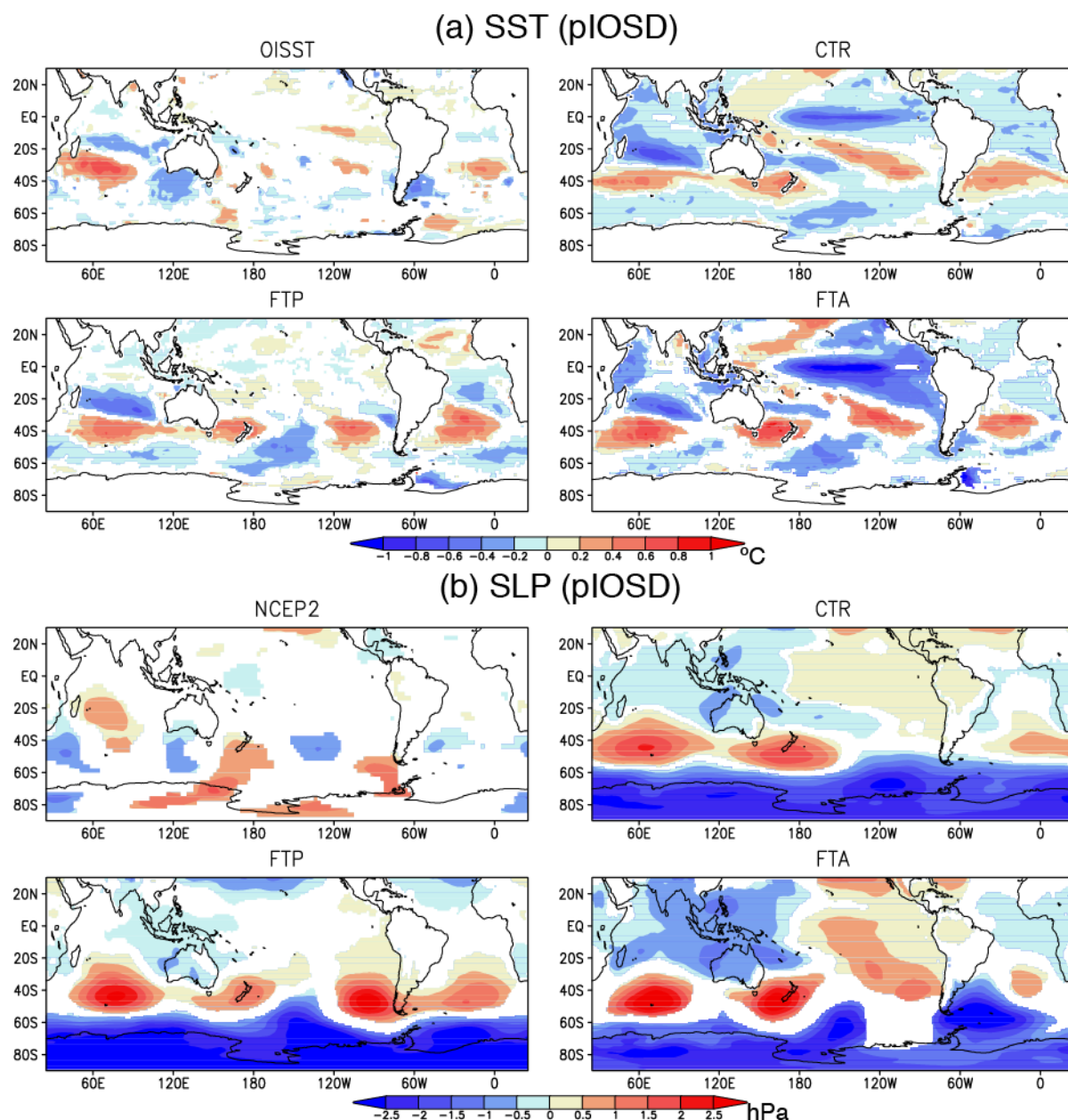


Figure 4: (a) Composite anomalies of SST (in °C) during austral summer of the positive IOSD for the observation (OISST) and CGCM (CTR, FTP, and FTA) experiments. (b) As in (a), but for the SLP (in hPa) during Nov.(0)-Jan.(1). For comparison, NCEP Reanalysis-2 (NCEP2) are shown. Anomalies exceeding the 90% (95%) confidence level by two-tailed t-test are shown for the observation, FTP, and FTA experiments (CTR experiment).

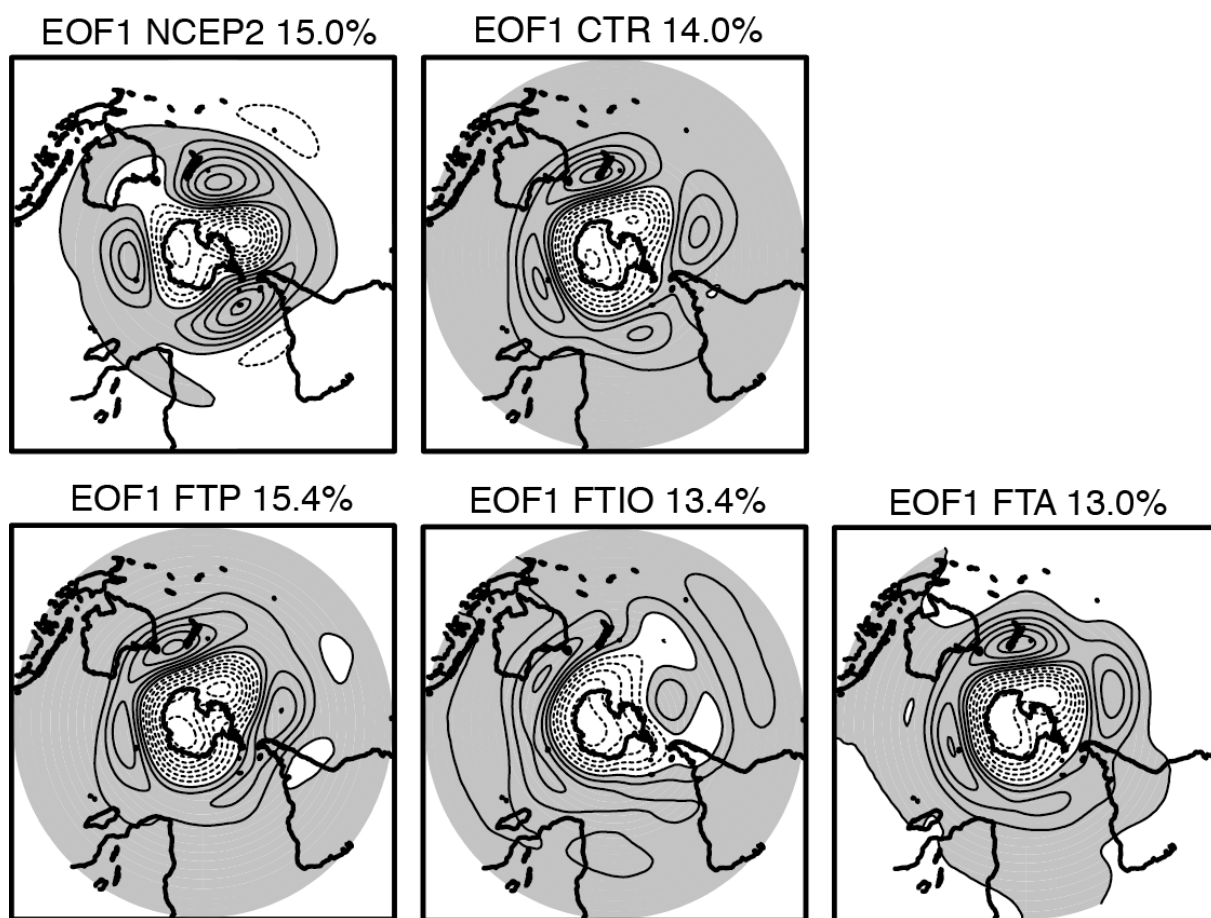


Figure 5: Spatial patterns of the first EOF mode of the geopotential height anomalies at 250 hPa (contour interval is 10 m). The NCEP Reanalysis-2 (NCEP2), the CGCM (CTR, FTP, FTIO, and FTA) experiments are shown, respectively. The positive values are shaded. Values on the top of the panel indicate the explained variance.

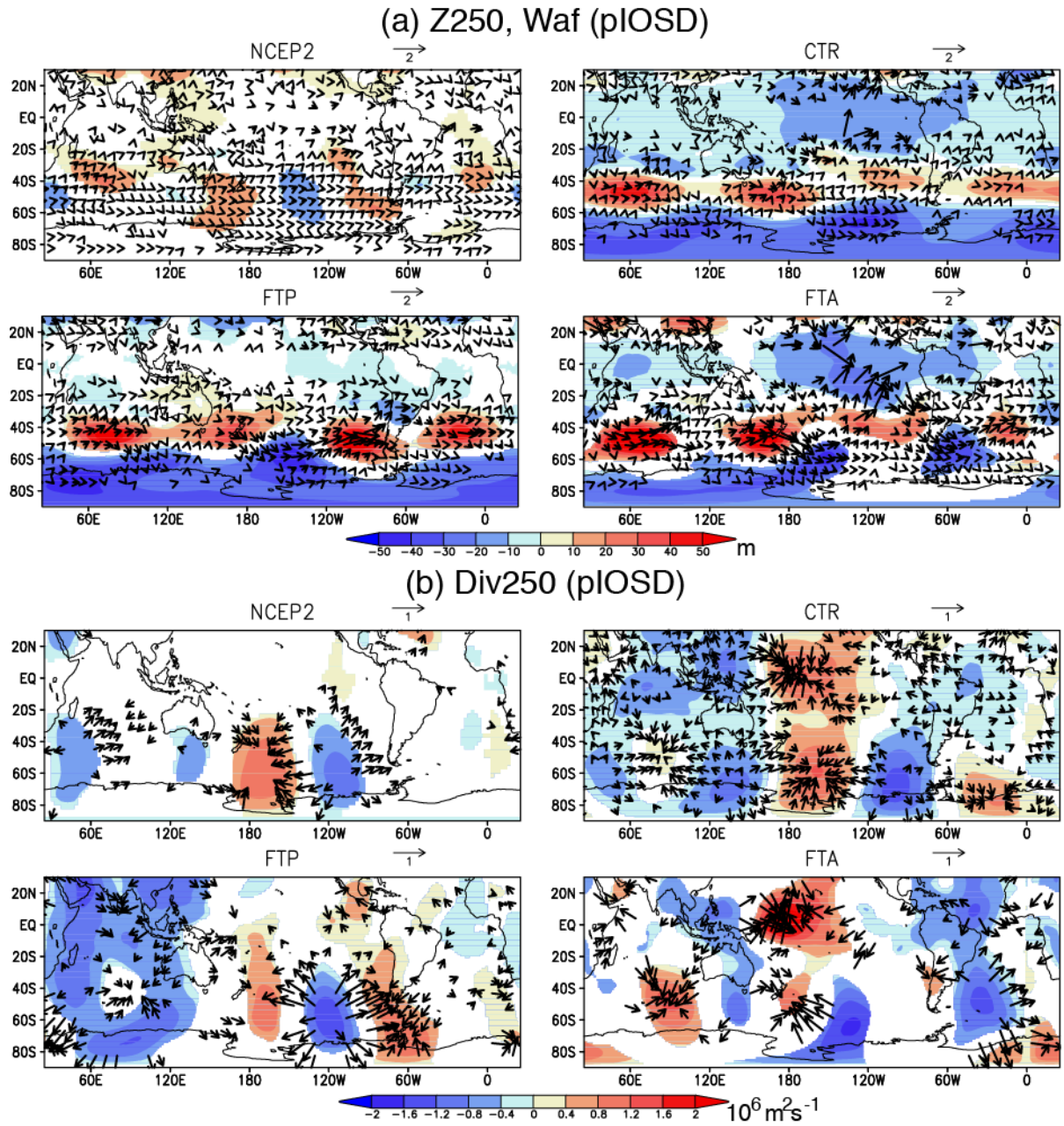


Figure 6: (a) As in Fig. 4b, but for the geopotential height at 250 hPa (color, in m) and wave activity flux (arrow, in $\text{m}^2 \text{s}^{-2}$). (b) As in (a), but for the velocity potential at 250 hPa (color, in $10^6 \text{m}^2 \text{s}^{-1}$) and divergent wind (arrow, in m s^{-1}).

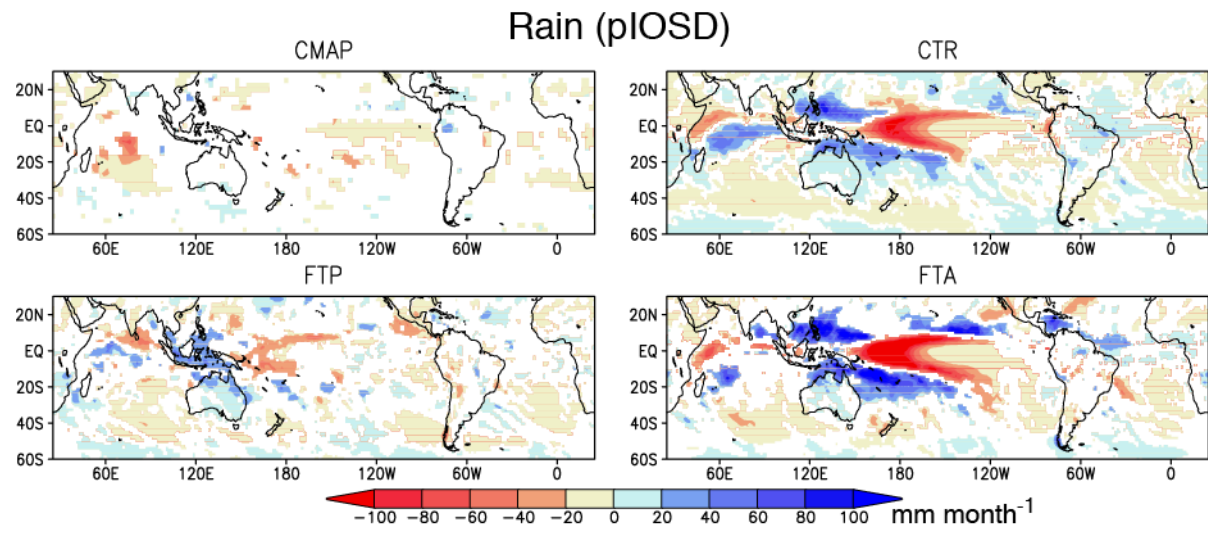


Figure 7: As in Fig. 4b, but for the rainfall (color, in mm month^{-1}).

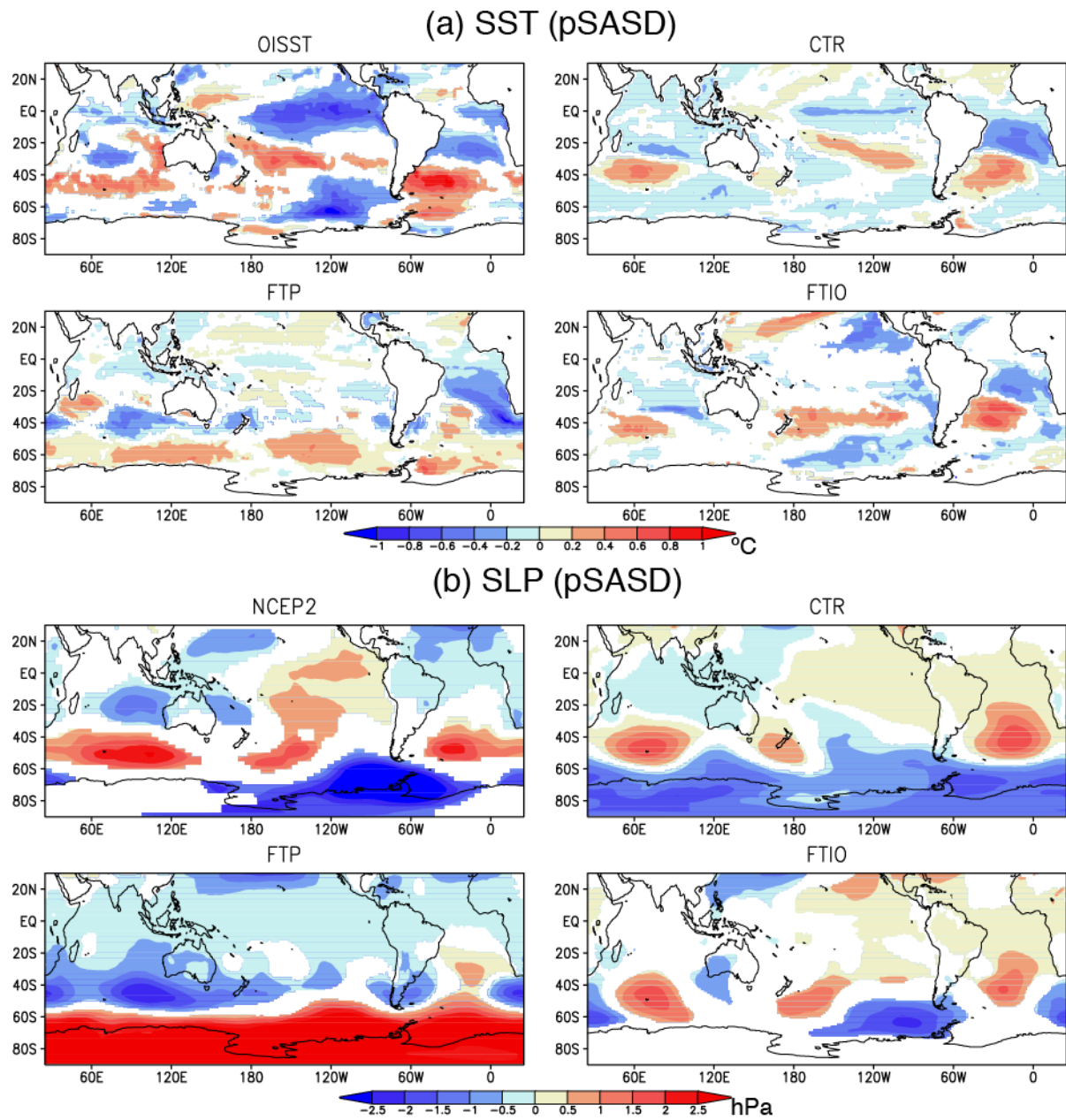


Figure 8: As in Fig. 4, but for the positive SASD. The FTP and FTIO experiments are shown.

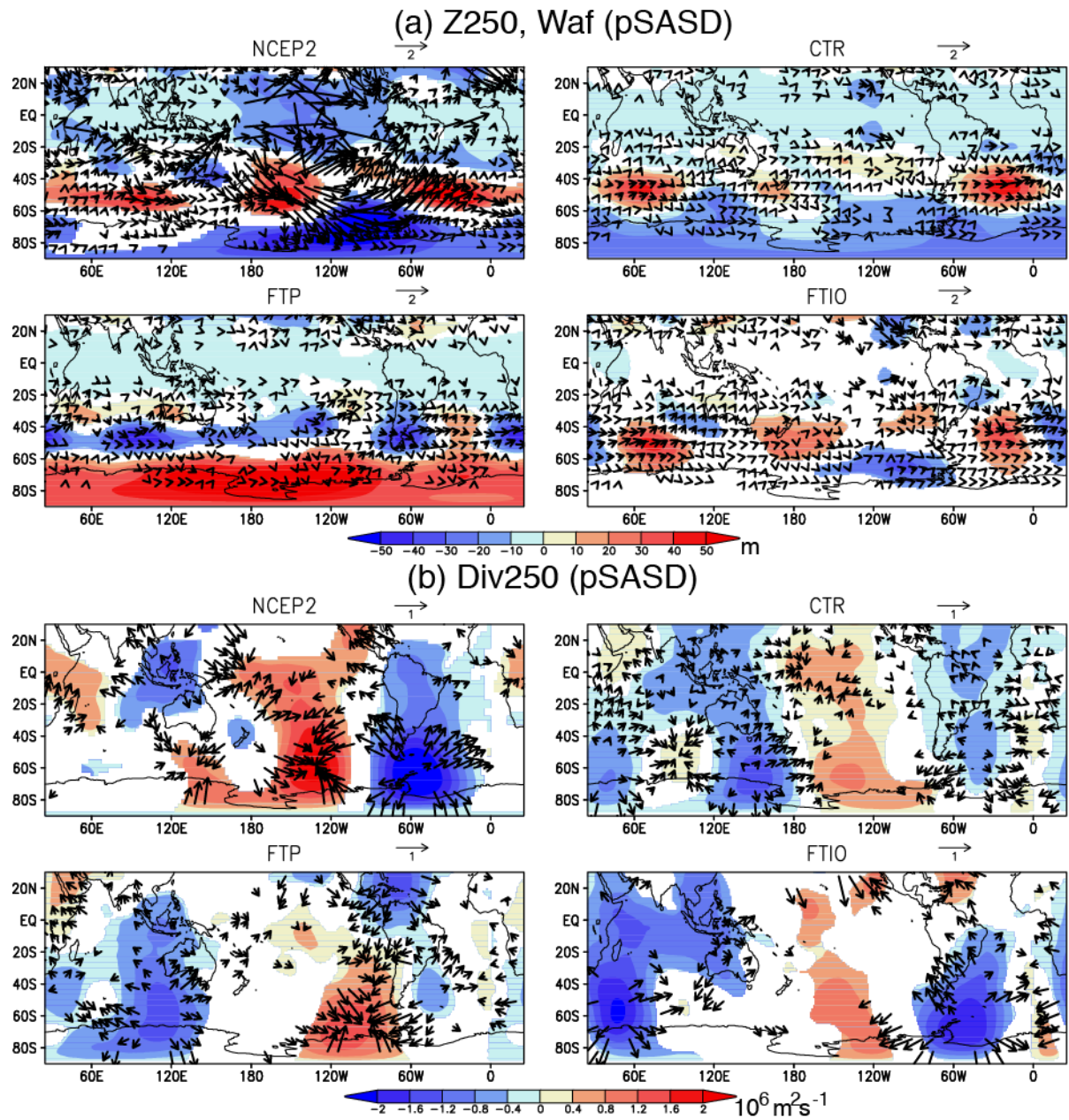


Figure 9: As in Fig. 6, but for the positive SASD. The FTP and FTIO experiments are shown.

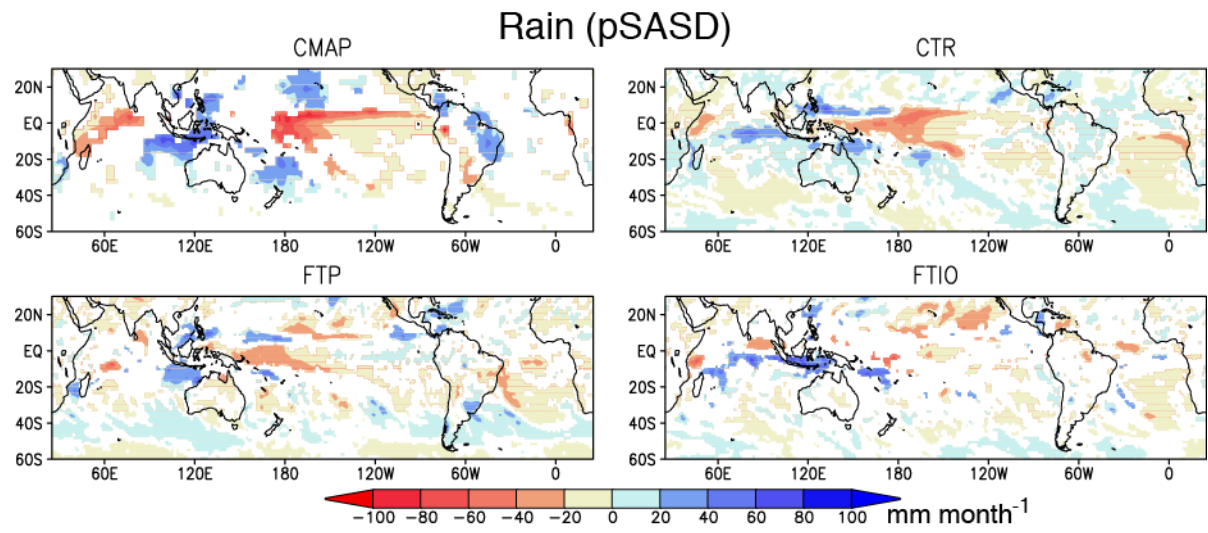


Figure 10: As in Fig. 7, but for the positive SASD. The FTP and FTIO experiments are shown.

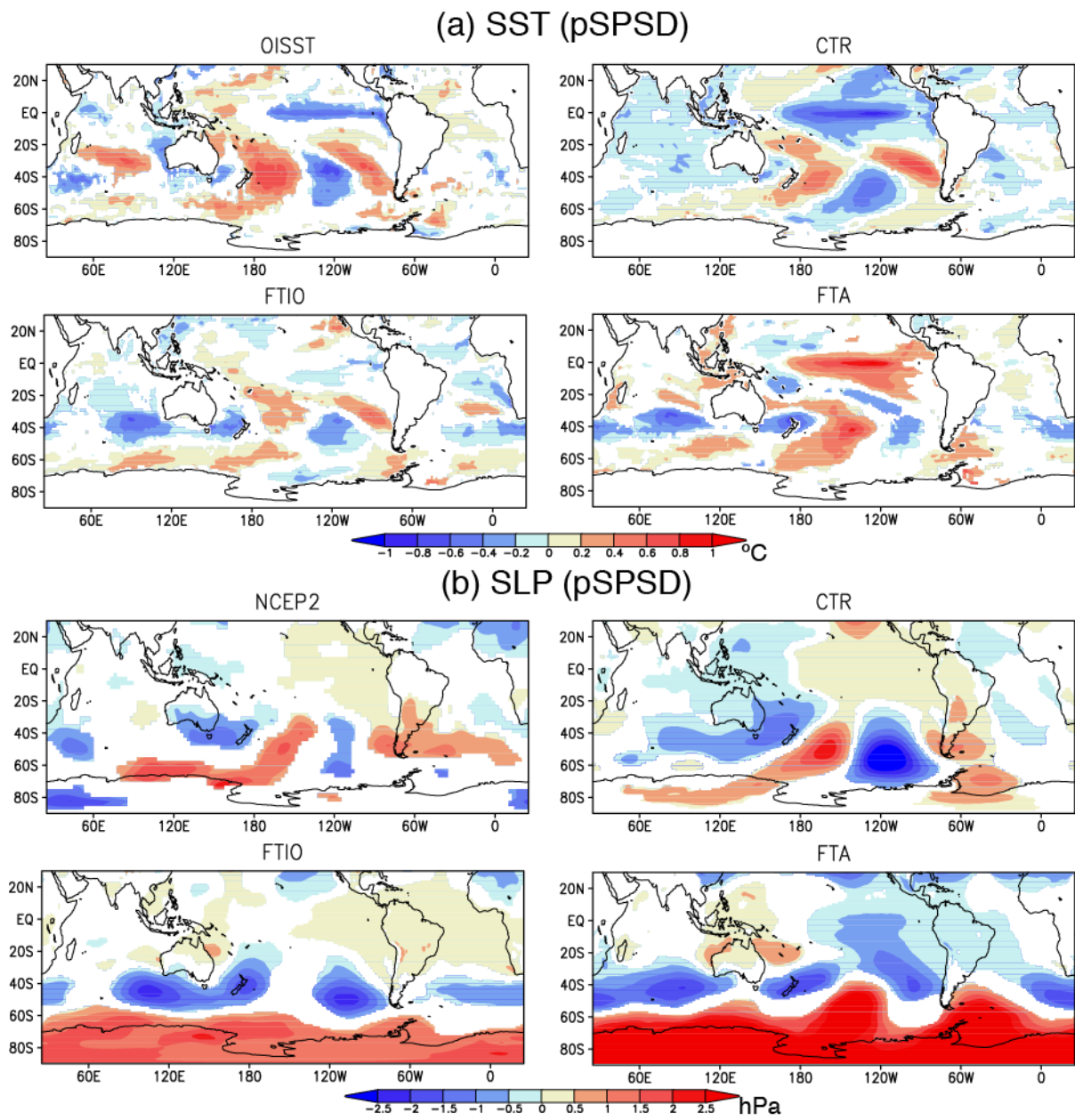


Figure 11: As in Fig. 4, but for the positive SPSD. The FTIO and FTA experiments are shown.

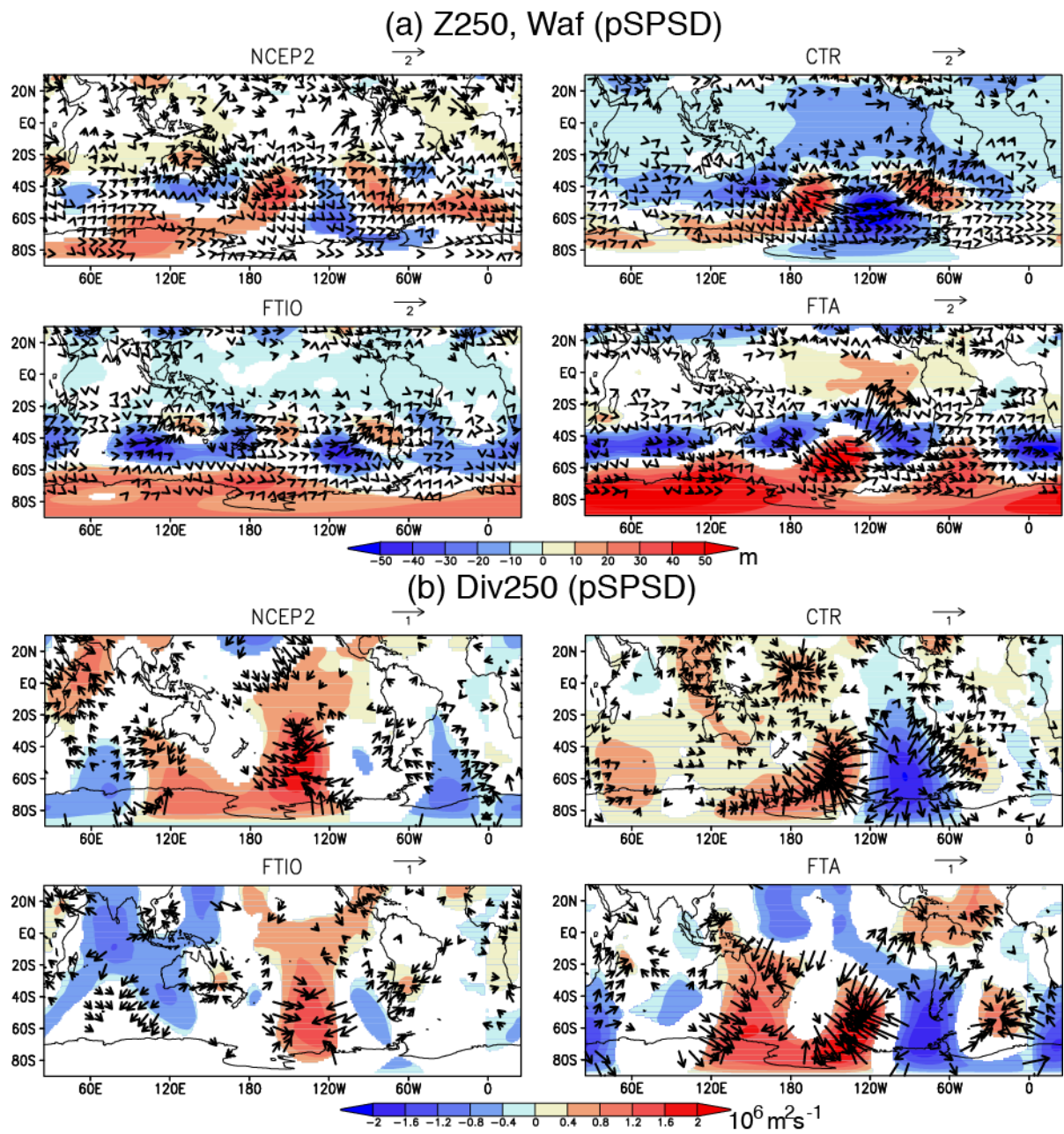


Figure 12: As in Fig. 6, but for the positive SPSPD. The FTIO and FTA experiments are shown.

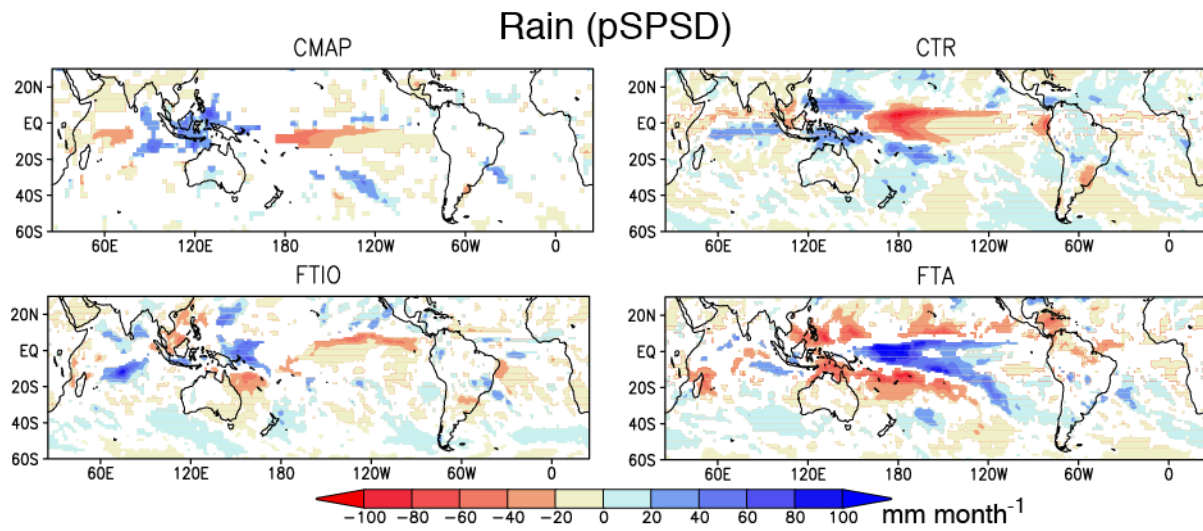


Figure 13: As in Fig. 7, but for the positive SPSD. The FTIO and FTA experiments are shown.

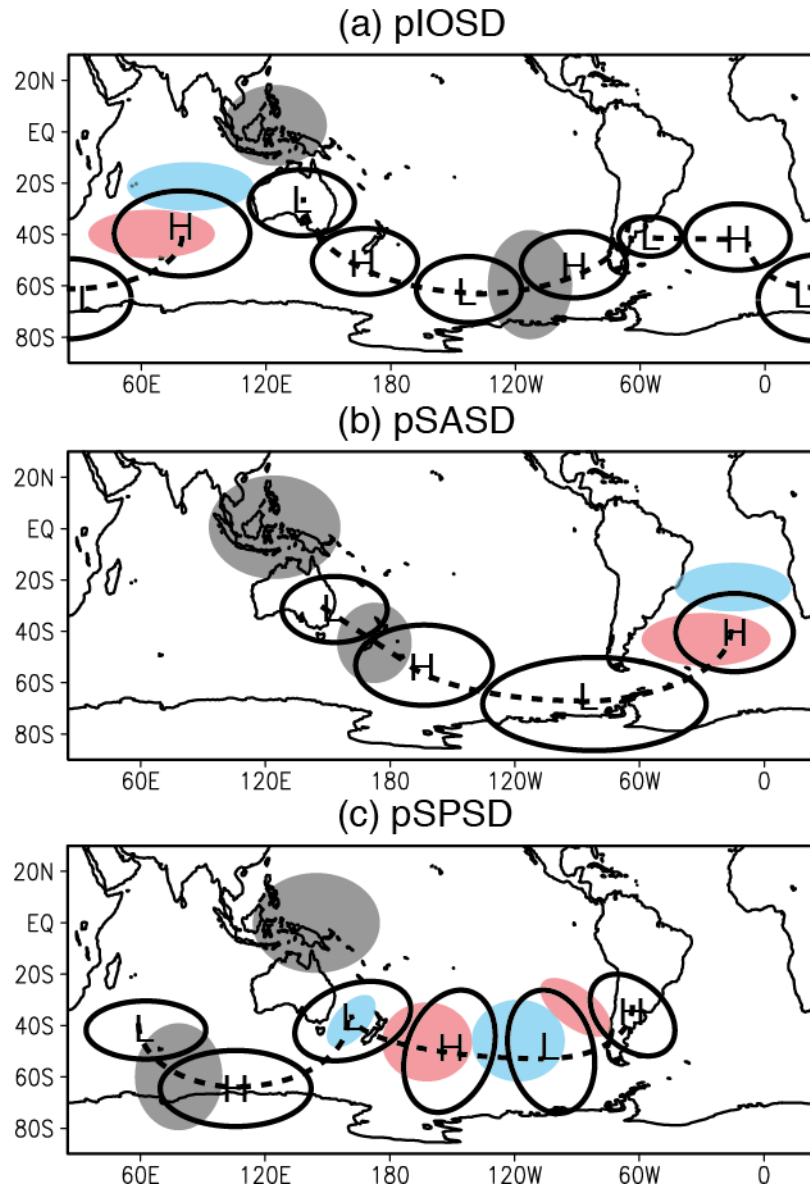
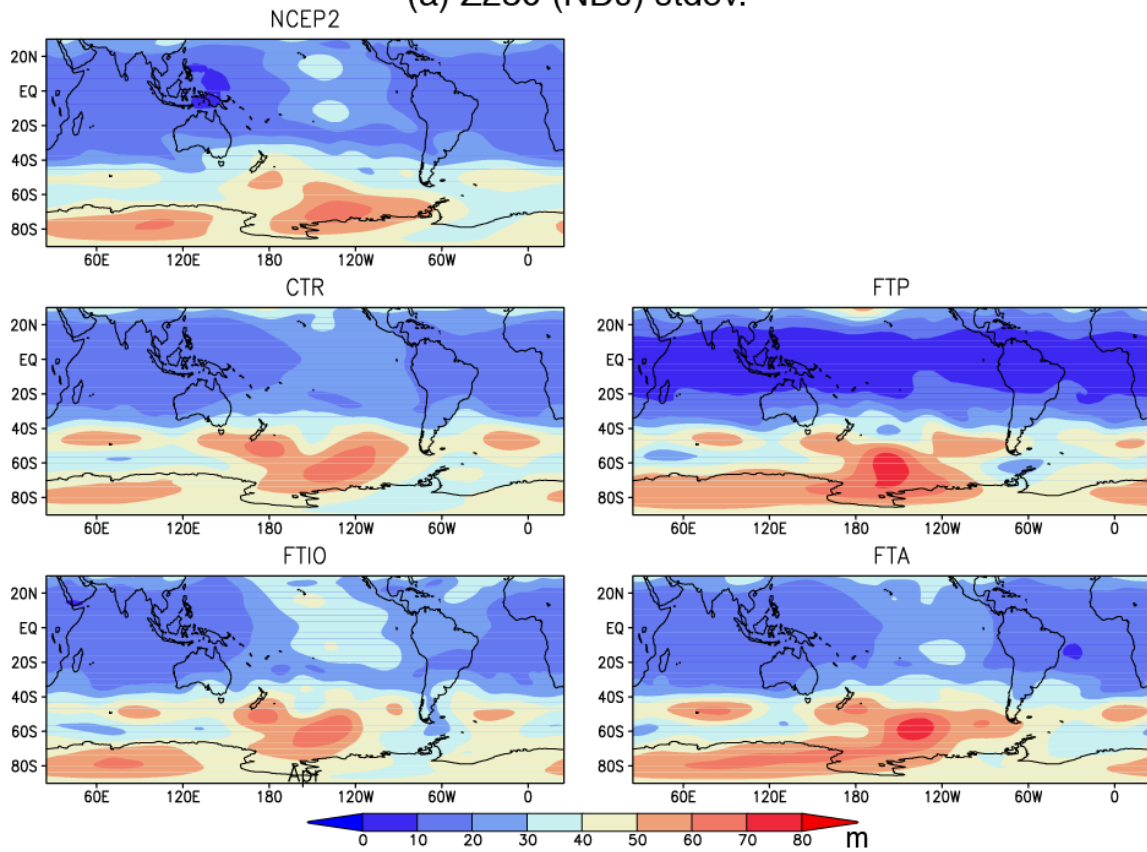


Figure 14: Schematic diagram illustrating the generation mechanism of the IOSD, SASD, and SPSPD derived from the reanalysis data and the CTR experiment. The warm (cold) color indicates the positive (negative) SST anomalies and the black shade indicates the anomalous wind divergence in the upper troposphere as potential sources of the Rossby waves. The dashed line shows the propagation pathway of the anomalous high (H) and low (L) pressure in the upper troposphere.

(a) Z250 (NDJ) stdev.



(b) Rain (NDJ) stdev.

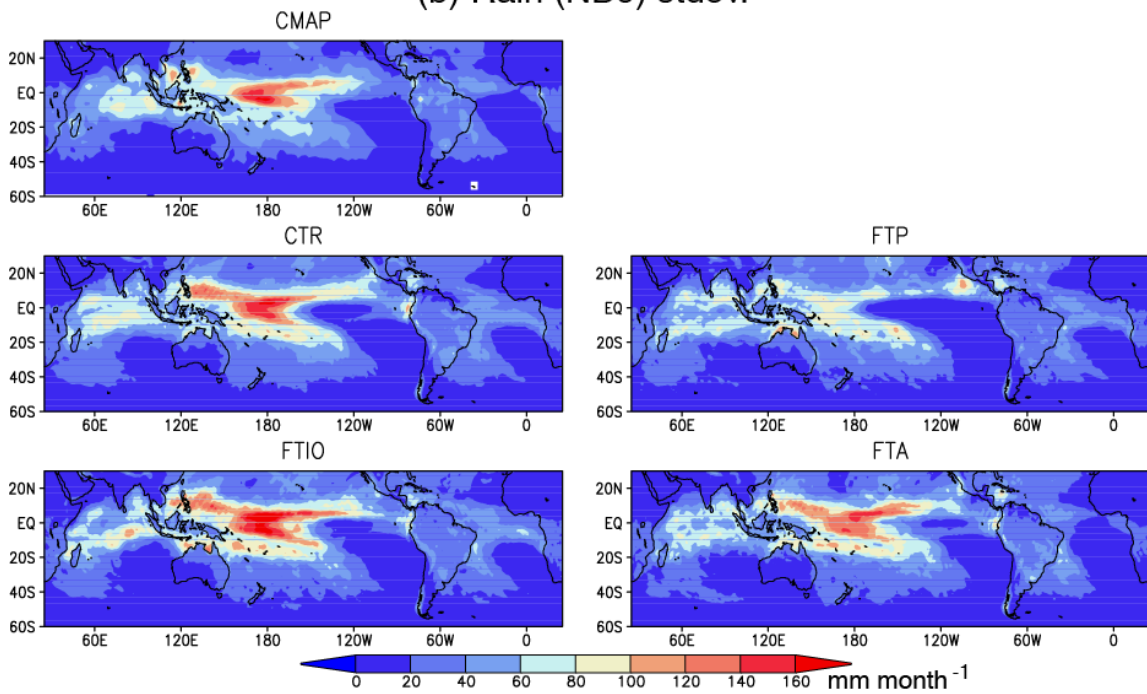


Figure 15: As in Fig. 1, but for (a) geopotential height at 250 hPa (in m) during Nov.-Jan.. (b) As in (a), but for the precipitation (in mm month⁻¹).